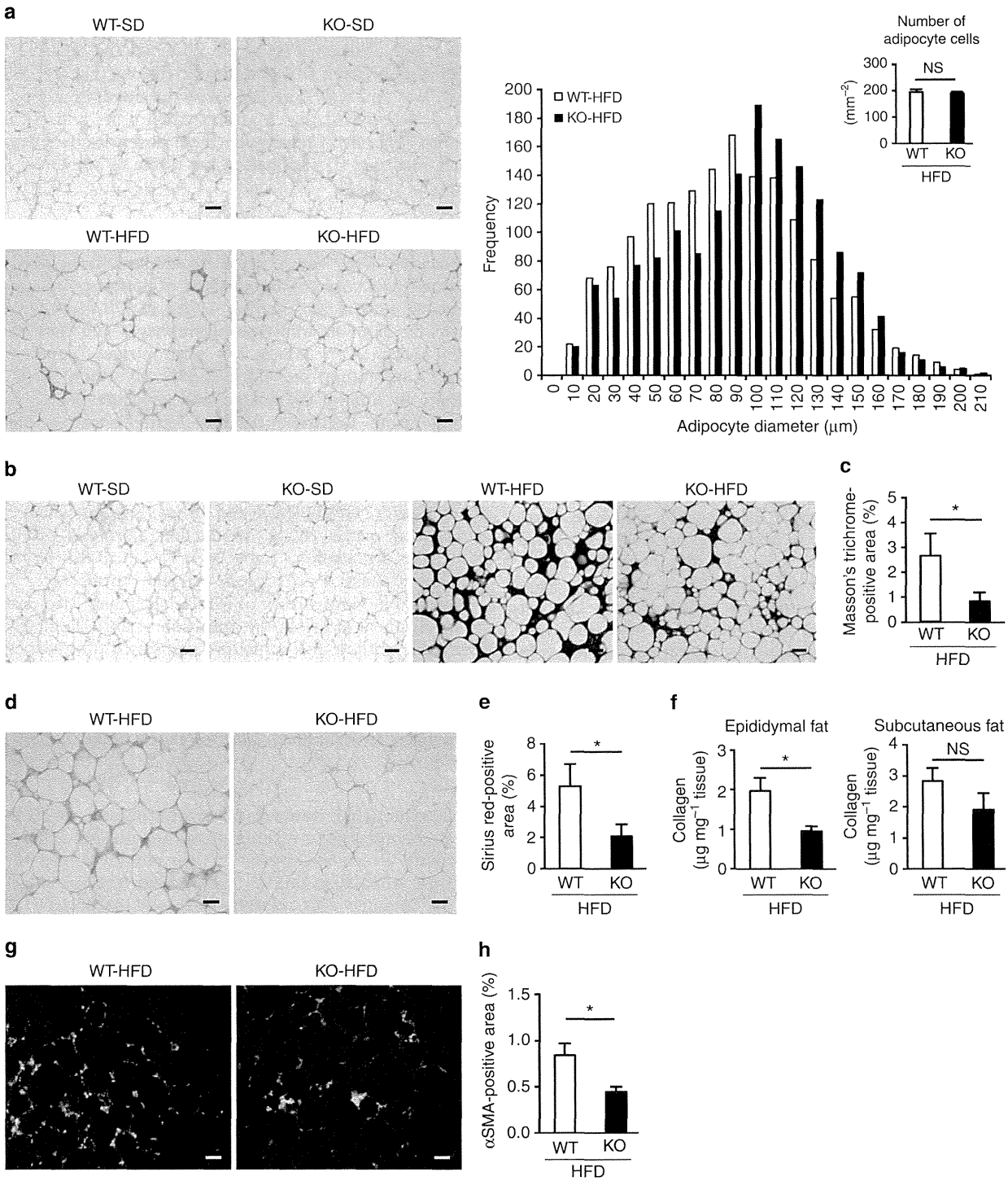

Figure 3 | Reduced interstitial fibrosis in adipose tissue of *Mincle* KO mice. *Mincle* KO and wild-type mice were fed a HFD or a SD for 16 weeks. (**a**) Representative hematoxylin and eosin staining, the histogram of adipocyte diameters in epididymal fat tissue. Inset, the number of adipocyte cells in epididymal fat tissue. (**b**,**c**) Representative Masson's trichrome staining (**b**) and quantification of Masson's trichrome-positive area (identical with *interstitial fibrosis*) (**c**) *in epididymal fat tissue*. (**d**,**e**) Representative Sirius red staining (**d**) *and quantification of Sirius red-positive area* (**e**) *in epididymal fat* tissue. (**f**) Total collagen contents in epididymal and subcutaneous fat tissues. (**g**,**h**) Representative αSMA staining (**g**) and quantification of αSMA-positive area (**h**) in epididymal fat tissue. Original magnification, × 200; Scale bar, 50 μm. Values are mean ± s.e.m. The data are analysed by unpaired *t*-test. $^*P<0.05$; NS, not significant; $n=11$ to 13.

fat tissue of *Mincle* KO and wild-type mice on a SD. Seven days after the injection, Masson's trichrome staining revealed extensive interstitial fibrosis in TDM-treated wild-type mice, which was markedly suppressed in TDM-treated *Mincle* KO mice (Fig. 7a,b). By immunofluorescent staining, TDM-treated wild-type mice exhibited the CLS formation, where macrophage-surrounding

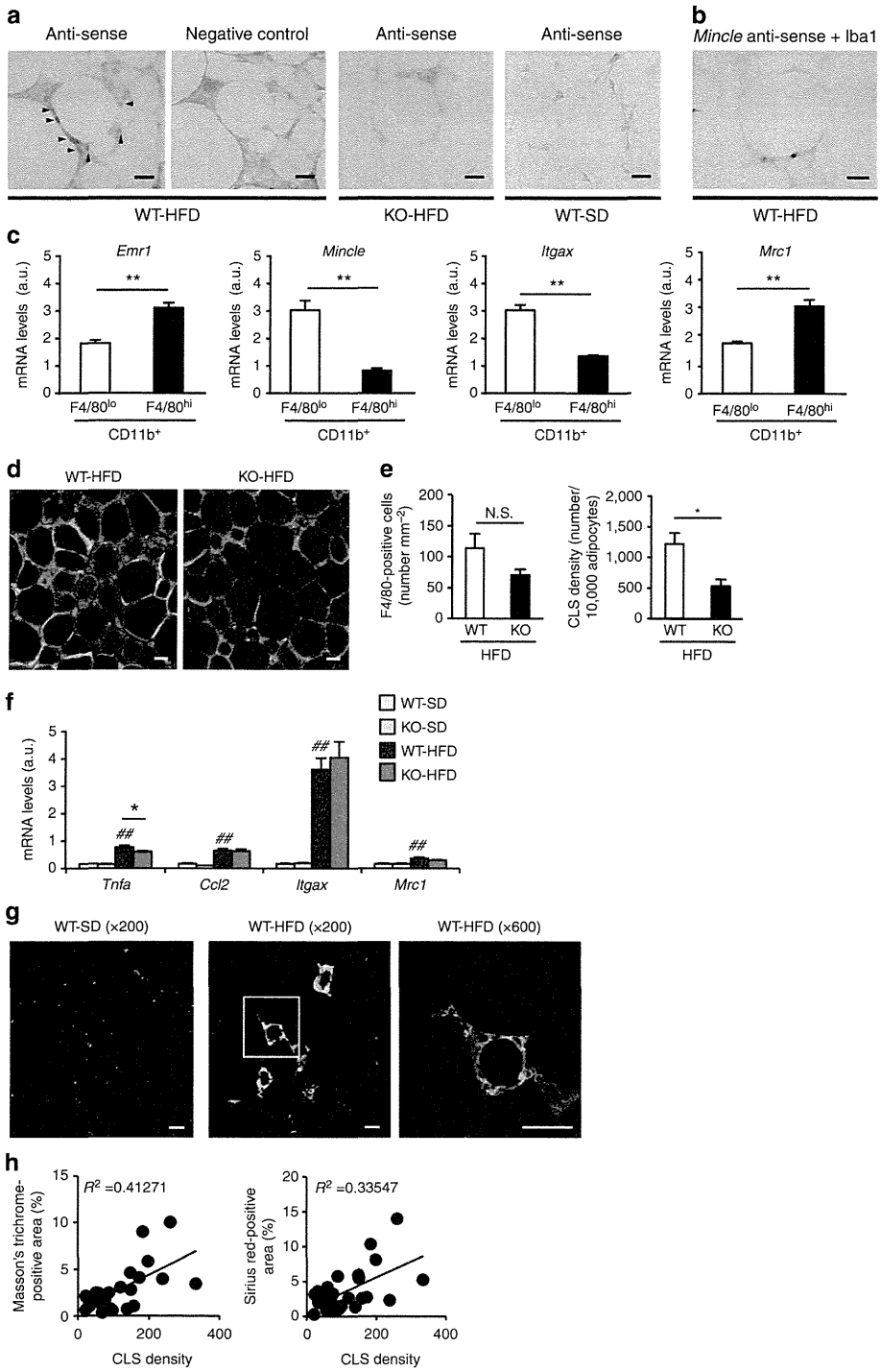

Figure 4 | Reduced CLS formation in adipose tissue of *Mincle* KO mice. (**a**) Representative *in situ* hybridization for *Mincle* mRNA in epididymal fat tissue of wild-type and *Mincle* KO mice fed a HFD for 16 weeks. The sections were hybridized with an anti-sense or a sense probe. (**b**) Double staining for *Mincle* (blue) and Iba1, a macrophage marker (brown). After *in situ* hybridization for *Mincle* mRNA, the sections were immunostained with an anti-Iba1 antibody. Original magnification, × 400; Scale bars, 25 μm. (**c**) mRNA expression of *Mincle*, *Emr1*, *Itgax* and *Mrc1* (CD206) in CD11b$^+$F4/80^{lo} and CD11b$^+$F4/80^{hi} cells isolated from SVF. Values are mean ± s.e.m. The data are analysed by unpaired *t*-test; $n=4$, $^{**}P<0.01$. (**d**,**e**) Representative immunofluorescent staining of F4/80 (red) and perilipin (green) (**d**) and the number of F4/80-positive cells and crown-like structure (CLS) density (**e**) in epididymal fat tissue of *Mincle* KO and wild-type mice fed a HFD for 16 weeks. Original magnification, × 200; Scale bars, 50 μm. Values are mean ± s.e.m. The data are analysed by unpaired *t*-test; $n=6$ to 8, $^{*}P<0.05$. NS, not significant. (**f**) mRNA expression of *Tnfa* (TNFα), *Ccl2* (MCP-1), *Itgax* and *Mrc1* in epididymal fat tissue of *Mincle* KO and wild-type mice fed a HFD for 16 weeks. Values are mean ± s.e.m. The data are analysed by ANOVA followed by Tukey–Kramer test. $n=5$ to 11. $^{\#\#}P<0.01$ versus WT-SD, $^{*}P<0.05$. (**g**) Representative immunofluorescent staining of F4/80 (green) and collagen I (red) in epididymal fat tissue of wild-type mice fed a SD or a HFD for 16 weeks. Scale bar, 50 μm. (**h**) Linear regression analysis of correlations between Masson's trichrome- or Sirius red-positive area and CLS density in epididymal fat tissue of wild-type mice fed a HFD for 16 to 20 weeks; $n=24$.

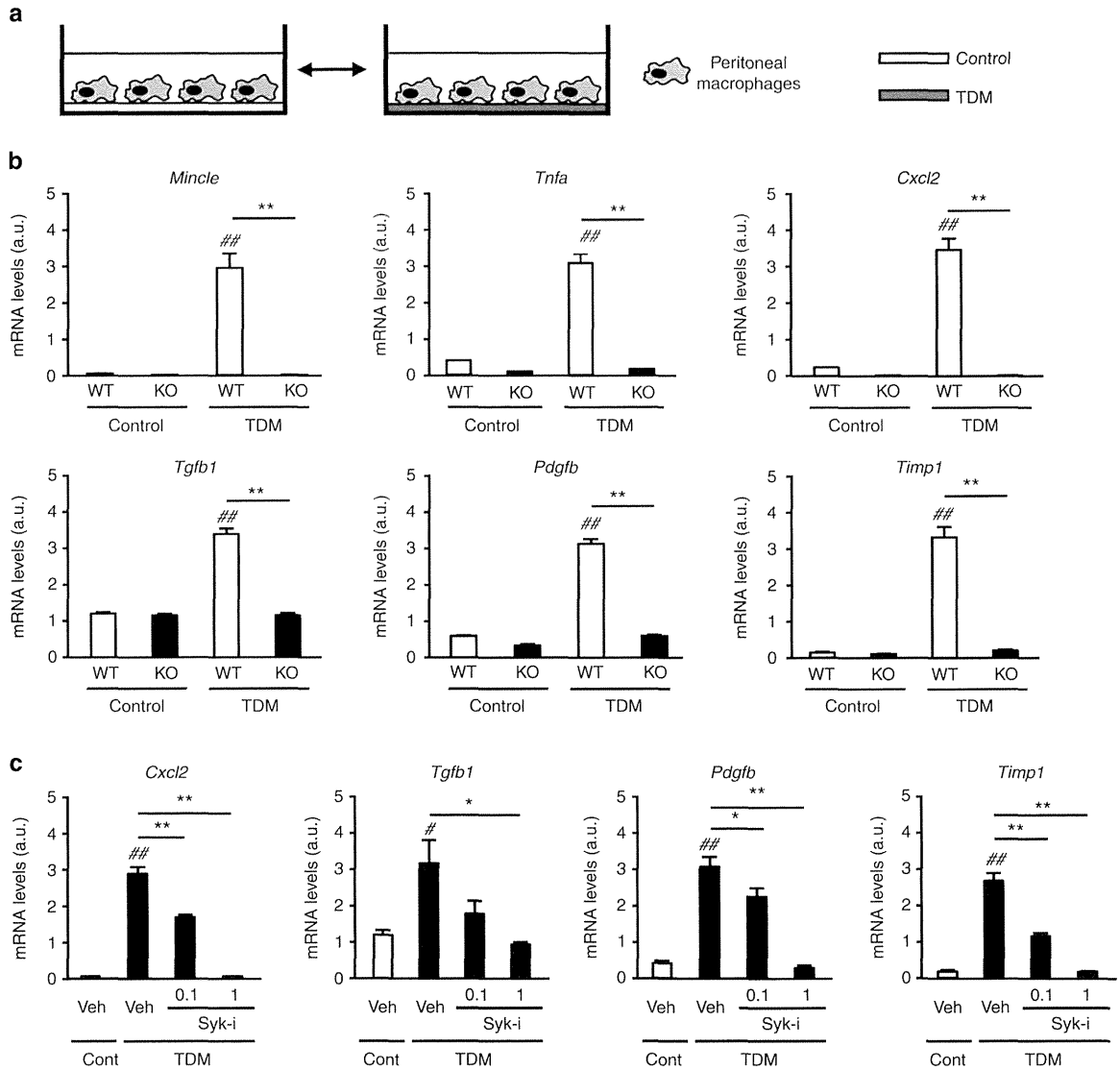

Figure 5 | Mincle-stimulated expression of fibrosis-related genes in macrophages. (**a**) Illustration of the TDM-stimulated experiments using peritoneal macrophages. (**b**) Effect of TDM stimulation for 24 h on mRNA expression of *Mincle*, inflammatory cytokines (*Tnfa* and *Cxcl2* (MIP-2)) and fibrosis-related genes (*Tgfb1* (TGFβ1), *Pdgfb* and *Timp1*) in peritoneal macrophages from *Mincle* KO and wild-type mice. (**c**) Effect of Syk-inhibitor BAY61-3606 (0.1, 1 μM) on mRNA expression in wild-type peritoneal macrophages stimulated with TDM. Cont, Control; Syk-i, Syk-inhibitor; TDM, trehalose-6,6′-dimycolate; Veh, Vehicle. Values are mean ± s.e.m. The data are analysed by ANOVA followed by Tukey-Kramer test; $n=4$, $^{\#}P<0.05$, $^{\#\#}P<0.01$ versus WT-Control or Veh-Control, $^{*}P<0.05$, $^{**}P<0.01$.

adipocytes were negative for perilipin staining, which was closely associated with collagen deposition (Fig. 7c). Moreover, we injected the emulsion into epididymal fat tissue of COL/EGFP transgenic (Tg) mice, which express EGFP exclusively in collagen I-producing cells. We observed that a number of EGFP-positive cells were accumulated around the CLS in TDM-treated mice (Fig. 7d). In TDM-treated wild-type mice, *Mincle* and *Itgax* mRNA expression was markedly induced throughout the experimental period, whereas *Mrc1* mRNA expression was gradually decreased (Fig. 7e). mRNA expression of *Acta2* and collagens was gradually increased up to day 7 (Fig. 7f). Notably, there was no upregulation of these genes in TDM-treated *Mincle* KO mice (Fig. 7f). Collectively, these observations suggest that Mincle stimulation is capable of inducing interstitial fibrosis in adipose tissue *in vivo*.

Discussion

Since numerous studies have shown that obesity induces chronic inflammation in adipose tissue[1,2], it is not surprising that, similar to various organs and tissues under chronic inflammation, adipose tissue exhibits interstitial fibrosis during the development of obesity. In line with this, recent evidence showed overproduction of extracellular matrix components in adipose tissue from obese animals and humans, which is implicated in systemic insulin resistance and hepatic steatosis[6,22–24]. However, little is known about how adipose tissue fibrosis is regulated in response to overnutrition. In this study, we provide evidence suggesting that Mincle is a novel regulator of adipose tissue fibrosis. Although macrophages are crucial for the regulation of tissue fibrosis, macrophages can promote and regress tissue fibrosis depending on the context[25].

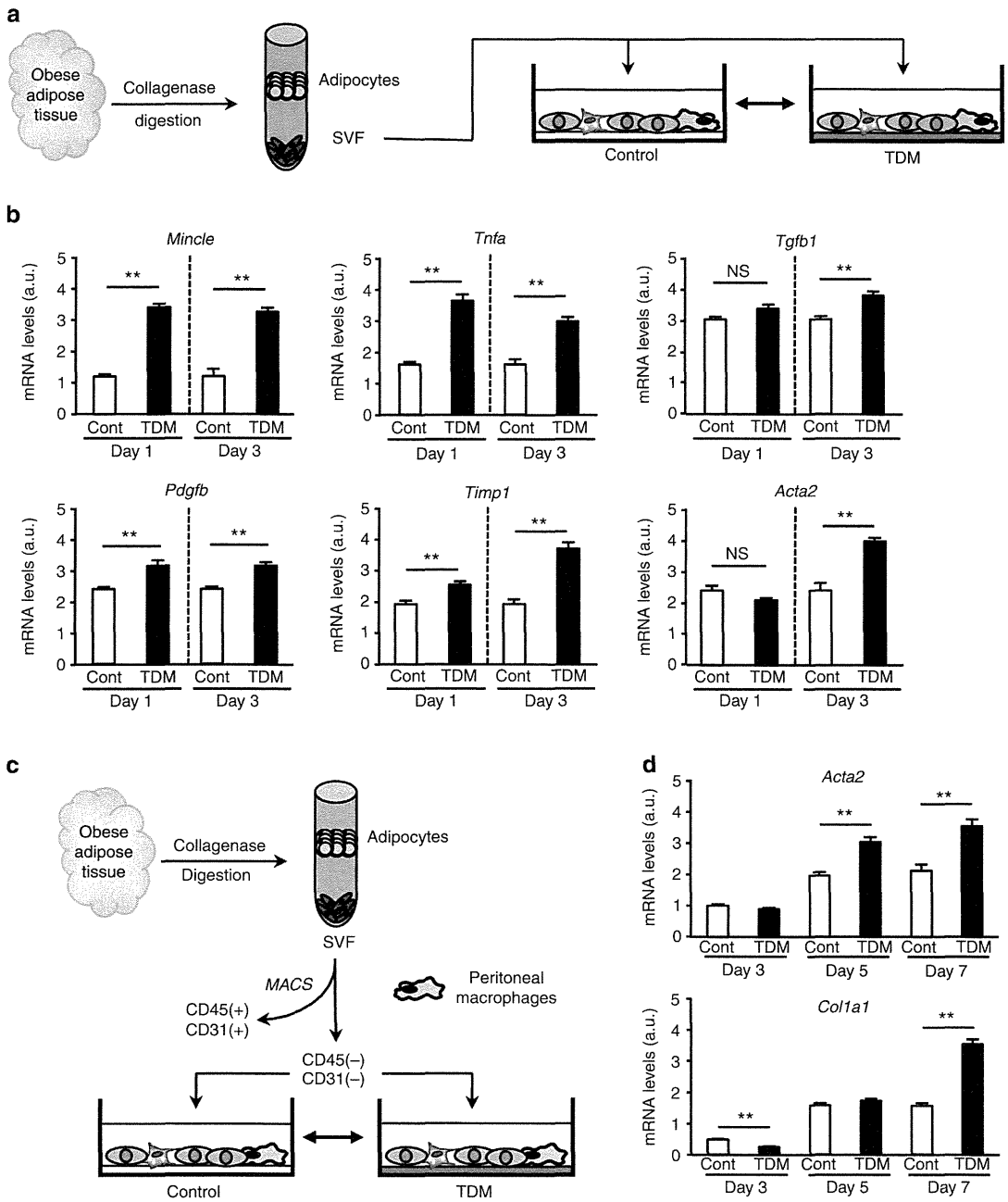

Figure 6 | Mincle-stimulated increase of myofibroblasts in SVF. (**a**) Illustration of the TDM-stimulated experiments using SVF. SVF prepared from epididymal fat tissue of *ob/ob* mice was stimulated with TDM for up to 3 days. (**b**) Effect of TDM stimulation on mRNA expression of *Mincle*, *Tnfa*, fibrosis-related genes (*Tgfb1*, *Pdgfb*, *Timp1*) and *Acta2*. Values are mean ± s.e.m. The data are analysed by unpaired *t*-test; $n=4$, $^{**}P<0.01$, NS, not significant. (**c**,**d**) Co-culture experiments of peritoneal macrophages and adipose tissue fibroblasts. (**c**) Illustration of the co-culture experiments using peritoneal macrophages and CD45$^-$CD31$^-$ cells in SVF, rich in fibroblasts, prepared from epididymal fat tissue of *ob/ob* mice using the magnetic cell sorting system (MACS). The cells were stimulated with TDM for up to 7 days. (**d**) Effect of TDM stimulation on mRNA expression of *Acta2* and *Col1a1* (collagen I). Values are mean ± s.e.m. The data are analysed by unpaired *t*-test; $n=4$, $^{**}P<0.01$.

Our data suggest that macrophages promote adipose tissue fibrosis through Mincle during the development of obesity.

We previously reported that a paracrine loop between adipocytes and macrophages establishes a vicious cycle that augments inflammatory changes in adipose tissue during the development of obesity[5]. CLS represents a unique structure where adipocytes and macrophages crosstalk in close proximity in obese adipose tissue *in vivo*, thereby accelerating adipose tissue inflammation. The data of this study suggest that CLS is an important origin of fibrosis as well as inflammation in adipose tissue. This notion is supported by our recent observations that the CLS-like histological structure in the liver of nonalcoholic steatohepatitis in mice and humans, which may be involved in the fibrogenesis of the liver[26]. Given that *Mincle* expression is localized to macrophages constituting CLS and that residual lipid droplets of dead adipocytes are scavenged by macrophages within CLS, Mincle can sense as-yet-unidentified endogenous ligands that are released as danger signals from dead adipocytes in the

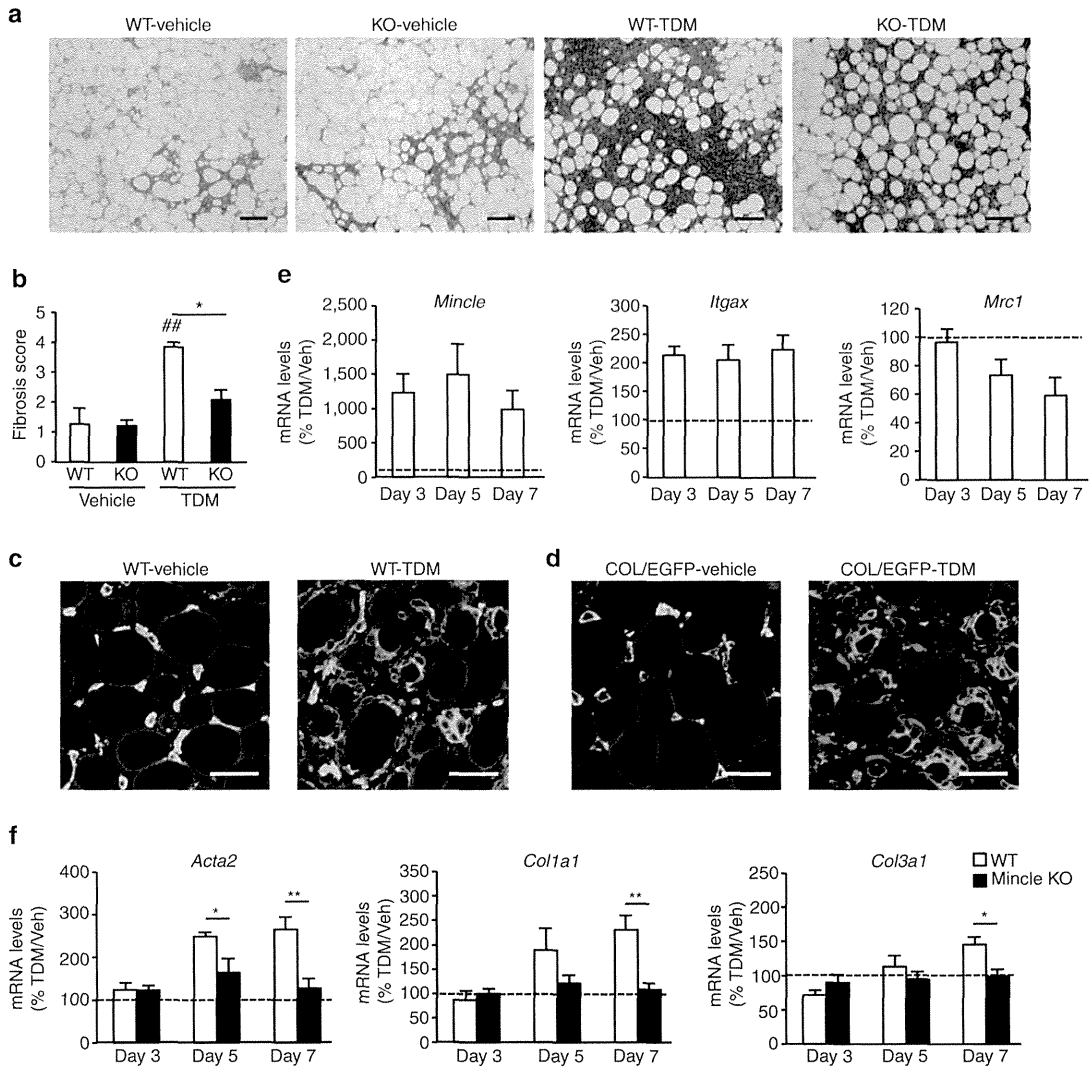

Figure 7 | Mincle-stimulated interstitial fibrosis in adipose tissue. Emulsion containing TDM or vehicle was injected into epididymal fat tissue of *Mincle* KO and wild-type mice. (**a**,**b**) Representative Masson's trichrome staining (**a**) and semiquantitative analysis of interstitial fibrosis (**b**) of epididymal fat tissue 7 days after injection. Original magnification, ×100; Scale bar, 100 μm. Values are mean ± s.e.m. The data are analysed by ANOVA followed by Tukey–Kramer test; $n=4$ to 5, $^{\#\#}P<0.01$ versus WT-vehicle, $^{*}P<0.05$. (**c**) Representative immunofluorescent staining of F4/80 (green), perilipin (blue) and collagen I (red) in wild-type mice treated with TDM or vehicle. Original magnification, ×600; Scale bar, 50 μm. (**d**) Representative immunofluorescent staining of F4/80 (green), perilipin (blue) and EGFP (red) in COL/EGFP Tg mice treated with TDM or vehicle. Original magnification, ×600; Scale bar, 50 μm. (**e**,**f**) Time course of mRNA expression up to 7 days after injection. mRNA expression of *Mincle*, *Itgax* and *Mrc1* in wild-type mice (**e**) and that of *Acta2*, *Col1a1* and *Col3a1* (collagen III) in *Mincle* KO and wild-type mice (**f**). Values are mean ± s.e.m. The data are analysed by unpaired *t*-test; $n=4$ to 5, $^{*}P<0.05$, $^{**}P<0.01$.

interaction between adipocytes and macrophages. This is the first report to elucidate the role of Mincle, a pathogen sensor for pathogenic fungi and *Mycobacterium tuberculosis*, in sterile inflammation. Considering the structural and functional similarities between CLS and mycobacterial granuloma, it is interesting to compare the role of Mincle under those conditions. In this regard, our data indicate the critical role of Mincle in CLS formation in adipose tissue, which is reminiscent of the recent report by Ishikawa *et al.* that Mincle is essential for the TDM-induced granuloma formation in lung[13]. Moreover, CLS in adipose tissue and granuloma structure in lung are accompanied by tissue fibrosis. Taken together, it is conceivable that Mincle has a role in metabolic stress- as well as pathogen-induced sustained cell-to-cell communication within CLS, thereby contributing to tissue remodelling.

It is important to know how Mincle-expressing macrophages are involved in fibrogenesis in adipose tissue. Stimulation of Mincle with TDM activates Syk in macrophages to increase expression of fibrosis-related genes as well as proinflammatory cytokines. These observations are consistent with previous studies that activation of Syk can induce TGFβ production in macrophages and dendritic cells[27,28]. On the other hand, *Mincle* is selectively expressed in proinflammatory M1 macrophages and localized to some of the macrophages constituting CLS in obese adipose tissue, whereas antiinflammatory M2 macrophages, not M1 macrophages, are considered to contribute to tissue repair and remodelling. These observations led us to speculate that Mincle-expressing macrophages could be a novel subpopulation of adipose tissue macrophages contributing to tissue remodelling under chronic inflammatory conditions. This notion is supported

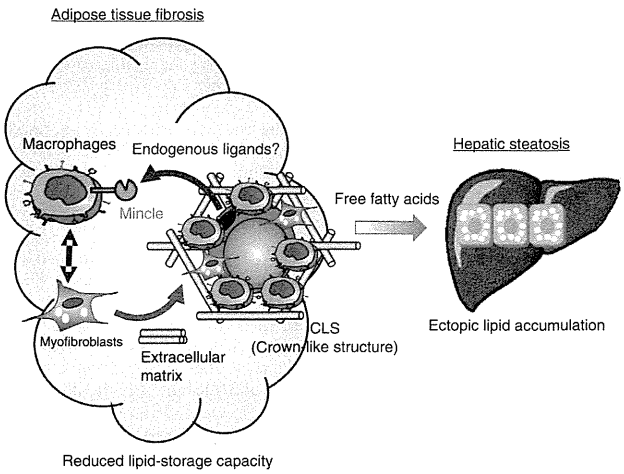

Figure 8 | Potential role of Mincle in obesity-induced adipose tissue inflammation. During the development of obesity, Mincle expression is induced in infiltrated macrophages and activated by an endogenous ligand released from dying adipocytes. Mincle is involved in macrophage aggregation to form CLS, and Mincle activation also induces expression of fibrosis-related genes thereby leading to myofibroblast formation. As a result, overproduction of ECM may limit the HFD-induced hypertrophy of adipocytes, which has a role in lipid accumulation in the liver and glucose intolerance.

by recent evidence that adipose tissue macrophages exhibit mixed phenotypes of M1 and M2 in obese humans and mice[29–31]. Interestingly, our data show that Mincle contributes to CLS formation and fibrogenesis without affecting macrophage polarization in obesity-induced adipose tissue inflammation. Since *Mincle* expression is quite low in adipose tissue from healthy lean mice, it is conceivable that Mincle-expressing macrophages are involved in pathological tissue remodelling in adipose tissue.

Fibrogenesis is a complex process caused by a variety of cells including myofibroblasts, immune cells and parenchymal cells. In terms of adipose tissue fibrosis, it is known that expression of collagen I and III is largely derived from SVF rather than adipocytes[32]. However, little is known about myofibroblasts in adipose tissue. In addition, myofibroblasts are derived from different cell types such as resident fibroblasts and fibrocytes, depending upon organs and tissues[20]. In this study, we observed increased number of αSMA-positive cells or myofibroblasts in obese adipose tissue. It is, therefore, interesting to know the origin of myofibroblasts in obese adipose tissue. In this regard, human preadipocytes are reported to be a source of ECM[33–35]. It is also important to understand the molecular mechanisms underlying myofibroblast formation during the development of obesity. Our data suggest that Mincle stimulation in macrophages effectively increases myofibroblast formation in SVF probably through the interaction between macrophages and fibroblasts. Consistently, several studies point to the role of macrophages in promoting fibroblastic phenotype and ECM production in human preadipocytes[33–35]. Taken together with recent observations that activation of hypoxia-inducible factor-1 in adipocytes contributes to interstitial fibrosis in adipose tissue[8], Mincle in macrophages may link obesity-induced adipocyte damages with myofibroblast formation.

Storing excessive energy as triglyceride is a fundamental function of adipose tissue. In response to nutritional conditions, lipid metabolism in adipose tissue is tightly regulated by hormones and the sympathetic nervous system. For instance, catecholamines induce adipocyte lipolysis to supply free fatty acids as fuel to other organs during the fasted state. On the other hand, insulin suppresses adipocyte lipolysis and facilitates lipogenesis in adipose tissue during the fed state[3]. In addition, accumulating evidence suggests that chronic inflammation in adipose tissue can induce ectopic lipid accumulation through several mechanisms[3,4]. First, obesity-induced chronic inflammation causes insulin resistance in adipose tissue[1,2]. Second, proinflammatory cytokines such as TNFα can directly induce lipolysis in adipocytes[5]. Finally, adipose tissue fibrosis may limit the expandability of adipose tissue during the development of obesity[6]. Divoux *et al.*[32] reported that adipose tissue fibrosis is negatively correlated with adipocyte diameters in human adipose tissue. It is also known that adipose tissue macrophage infiltration is associated with hepatic lipid accumulation in humans[36]. Moreover, we observed that melanocortin 4 receptor-deficient mice fed a HFD exhibit accelerated adipose tissue inflammation with interstitial fibrosis, which may contribute to excessive lipid accumulation in the liver[24]. In line with this, *Mincle* KO mice are protected against obesity-induced adipose tissue fibrosis and ectopic lipid accumulation in the liver. We also found that serum FFA concentrations are significantly decreased in *Mincle* KO mice relative to wild-type mice. All these data support the notion that increased lipid-storage capacity of adipose tissue in *Mincle* KO mice may cause less efflux of FFA from adipose tissue to the liver. Our data highlight the role of Mincle as a novel mechanism of how chronic inflammation induces ectopic lipid accumulation in obesity.

It is important to know which organ is responsible for the ameliorated glucose tolerance in *Mincle* KO mice. In this study, *Mincle* KO mice exhibit better glucose tolerance and lower serum insulin concentrations than wild-type mice as early as 16 weeks after HFD feeding, when there is a marked reduction of hepatic steatosis in *Mincle* KO mice. Consistently, insulin sensitivity is significantly increased in the liver and tends to be ameliorated in adipose tissue and skeletal muscle as well as in *Mincle* KO mice relative to wild-type mice. These observations support the notion that activation of Mincle in adipose tissue triggers ectopic lipid accumulation and insulin resistance in the liver, thereby inducing systemic glucose intolerance. On the other hand, we do not exclude the possibility that Mincle in non-adipose tissues has a role in obesity-induced ectopic lipid accumulation and insulin resistance, since obesity also induces *Mincle* expression in liver to a lesser extent than adipose tissue. Further studies are required to elucidate the molecular mechanisms underlying Mincle-mediated glucose intolerance in obesity.

On the basis of our observations, we hypothesize a role of Mincle in adipose tissue inflammation in obesity as follows (Fig. 8). During the development of obesity, Mincle expression is induced mainly through TLR4 in infiltrated macrophages as we previously reported[18]. Activated by an endogenous ligand released from dying adipocytes, Mincle is involved in macrophage aggregation to form CLS, where there is a sustained interaction between adipocytes and macrophages. Mincle activation also induces expression of fibrosis-related genes through Syk, thereby leading to myofibroblast formation possibly through intercellular communication between macrophages and fibroblasts. As a result, overproduction of ECM may limit the HFD-induced hypertrophy of adipocytes, which has a role in lipid accumulation in the liver and glucose intolerance.

In summary, we demonstrated in this study that Mincle has a critical role in HFD-induced CLS formation and adipose tissue fibrosis, which may reduce lipid-storage capacity in adipose tissue and enhance ectopic lipid accumulation. Our data also suggest that Mincle in macrophages would be a novel therapeutic target to prevent or treat obesity-induced adipose tissue inflammation and metabolic derangement.

Methods

Reagents. All reagents were purchased from Sigma-Aldrich (St Louis, MO) or Nacalai Tesque (Kyoto, Japan) unless otherwise noted.

Animals. The *Mincle* KO mice and enhanced green fluorescence protein (*Egfp*) Tg mice on the C57BL/6J genetic background were kindly provided by Drs Shizuo Akira and Masaru Okabe (Osaka University)[16,37], respectively. We crossed these mice to generate the *Mincle* KO-*Egfp* Tg mice for the BMT experiments. Eight-week-old C57BL/6J-*ob/ob* and wild-type mice were purchased from Japan SLC (Shizuoka, Japan). They were maintained in a temperature-, humidity- and light-controlled room (12 h light/dark cycles), allowed free access to water and standard chow (CE-2; 343.1 kcal per 100 g, 12.6% energy as fat; CLEA Japan, Tokyo, Japan). Ten-week-old animals were fed either an SD (CE-2) or HFD (D12492; 556 kcal per 100 g, 60% energy as fat; Research Diets, New Brunswick, NJ) for 8, 16 and 50 weeks. The COL/EGFP Tg mice on the C57BL/6J background, which express EGFP exclusively in collagen I-producing cells, were used to detect myofibroblasts[38]. All animal experiments were approved by the Institutional Animal Care and Use Committee of Tokyo Medical and Dental University (No.2011-207C, No.0140016A). We used male 9–11-week-old mice with a C57BL/6J background in all experiments in the present study unless otherwise noted.

Histological analysis. The epididymal fat tissue and liver were fixed with neutral-buffered formalin and embedded in paraffin. Two-micrometre thick sections were stained with hematoxylin and eosin, Masson's Trichrome, or Sirius red. For the measurement of adipocyte cell size, more than 200 cells were counted per each section using an image analysis software (WinRoof; Mitani, Tokyo, Japan). Fibrosis and αSMA-positive area were measured by an image analysis software (Dynamic Cell Count; Keyence, Osaka, Japan). The presence of F4/80-positive macrophages in epididymal fat tissue was detected immunohistochemically using the rat monoclonal anti-mouse F4/80 antibody kindly provided by Dr Motohiro Takeya (Kumamoto University)[39,40]. The number of F4/80-positive cells was counted in more than 10 mm^2 area of each section and expressed as the mean number per mm^2. The CLS density was obtained by counting the total numbers of CLS and adipocytes in each section, which was expressed as CLS number per 10,000 adipocytes[41]. Antibodies used in this study for immunohistochemistry are listed in Supplementary Table 2. To evaluate the TDM-induced adipose tissue fibrosis, the sections were graded semiquantitatively (scores 0 to 4) according to the Masson's trichrome-positive area (0 = none, 1 = weak, 2 = mild, 3 = moderate, 4 = severe). The representative histological images for the respective score values were shown in Supplementary Fig. 9. The quantitative histological analysis was performed by three investigators who had no knowledge of the origin of the slides.

***In situ* hybridization.** *In situ* hybridization for *Mincle* mRNA was performed as reported[42]. Paraffin-embedded tissue blocks from epididymal fat tissue were sectioned at 8 μm. The sections were fixed with 4% paraformaldehyde for 15 min, treated with 8 μg ml^{-1} proteinase K for 30 min at 37 °C, re-fixed with 4% paraformaldehyde and then acetylated with 0.25% acetic anhydride for 10 min. Hybridization was performed with probes at concentrations of 300 ng ml^{-1} at 60 °C for 16 h. After hybridization, the sections were washed in 5 × saline sodium citrate (SSC) at 60 °C for 20 min and then in 50% formamide and 2 × SSC at 60 °C for 20 min, followed by treatment with 50 μg ml^{-1} RNaseA for 30 min at 37 °C. After the sections were further washed several times with 2 × SSC and 0.2 × SSC, they were incubated with anti-DIG AP conjugate (Roche) for 1 h at room temperature. After washing twice, colouring reactions were performed with NBT/BCIP solution (Roche) overnight. Several sections were double stained with a macrophage marker, Iba1.

Flow cytometric analyses. Flow cytometric analyses of SVF were performed as described[43,44]. In brief, the epididymal fat tissue was collected and cut into small pieces and incubated for 20 min in collagenase solution (2 mg ml^{-1} of collagenase type 2 (Worthington, Lakewood, NJ)) with gentle shaking. After filtering though a 180-μm mesh, we centrifuged it and resuspended in phosphate-buffered saline (PBS). We washed the dissociated SVF twice with PBS, incubated them for 10 min in erythrocyte-lysing buffer and filtered it through a 70-μm mesh. Cells were sorted using FACSAriaII (BD Biosciences, San Jose, CA) and used for mRNA expression analysis. Mincle-expressing cells were analysed using FACSCantoII (BD Biosciences) and FlowJo 7.2.2. software (Tomy Digital Biology, Tokyo, Japan). Mincle-expressing cells were identified by anti-Mincle antibody (clone 4A9; MBL, Nagoya, Japan) labelled with Lightning-Link Atto-488 (Innova Biosciences, Cambridge, UK). Other antibodies used in flow cytometric analyses were listed in Supplementary Table 3.

Confocal microscopic analysis. For confocal microscopic analysis, isolated tissue pieces were fixed in 4% formaldehyde and permeabilized with 0.5% Triton X-100. The specimens were then blocked with 1% BSA and incubated with a pair of primary antibodies and then with the respective secondary antibodies. The stainings were examined by using the FluoView FV10i confocal microscope system (Olympus, Tokyo, Japan).

Collagen content in adipose tissue. Total collagen content in adipose tissue was measured using a commercially available kit (The QuickZyme total collagen assay; QuickZyme Biosciences, Leiden, Netherlands).

Triglyceride content in liver. Total lipids in the liver were extracted using ice-cold chloroform and methanol, 2:1 (v/v). Triglyceride content in the liver content was measured using an enzymatic assay kit (Wako Pure Chemical Industries, Osaka, Japan).

Glucose and insulin tolerance tests. Glucose tolerance test was performed after an 18-h fast. Blood glucose concentrations were measured at 0, 15, 30, 60, 90 and 120 min after intraperitoneal injection of glucose (2 g kg^{-1} body weight) by a blood glucose test meter (Glutest PRO R; Sanwa-Kagaku, Nagoya, Japan). For insulin tolerance test, insulin (0.5 U kg^{-1} body weight of Humulin R-Insulin; Eli Lilly, Indianapolis, IN) was injected intraperitoneally after a 1-h fast. Blood glucose concentrations were measured 0, 15, 30, 60, 90 and 120 min after the injection.

Western blotting of Akt. Western blotting was performed as described[45]. In brief, mice with food deprivation for 16 h were injected with insulin (0.5 U kg^{-1} body weight of Humulin R-Insulin; Eli Lilly) or PBS via the postcaval vein. Liver, soleus muscle and epididymal fat tissue were removed 1, 2 and 3 min after the injection, respectively. Immunoblotting was performed using anti-phospho-Akt (Thr308) antibody (Cell Signaling Technology, Danvers, MA) and anti-Akt antibody (Santa Cruz Biotechnology, Santa Cruz, CA). Immunoblot images were quantified using ImageQuant LAS 4000 mini (Fujifilm, Tokyo, Japan). Representative uncropped blots are shown in Supplementary Fig. 10.

Serum analysis. Serum FFA and ALT, and insulin concentrations were measured using a standard enzymatic assay or a commercially available enzyme-linked immunosorbent assay kit.

TDM stimulation. For stimulation of thioglycollate-elicited peritoneal macrophages or SVF from epididymal fat tissue of *ob/ob* mice, TDM dissolved in chloroform at 1 mg ml^{-1} were diluted in isopropanol and added on 12- or 48-well culture plates (5 or 1.25 μg of TDM per well, respectively), followed by evaporation of the solvent as described[13,46]. In some experiments, peritoneal macrophages were co-cultured with adipose tissue fibroblasts ($CD45^-CD31^-$ cells prepared from SVF of *ob/ob* mice using the magnetic cell sorting system (MACS; Miltenyi Biotec, Auburn, CA)). For *in vivo* experiments, the emulsion containing TDM (10 μg; ref. 13) was directly injected into epididymal fat tissue. Three, five and seven days after the injection, the epididymal fat tissue was collected and subjected to gene expression analysis and Masson's trichrome and immunofluorescent stainings.

Quantitative real-time PCR. Quantitative real-time PCR was performed as described[18]. In brief, total RNA was extracted from the tissues or cultured cells using Sepasol reagent and 10 ng of cDNA was used for real-time PCR amplification with SYBR GREEN detection protocol in a thermal cycler (StepOne Plus, Applied Biosystems, Foster City, CA). Primers used in this study are listed in Supplementary Table 4. Data were normalized to the *36B4* levels, and analysed using the comparative CT method.

Microarray analysis. Microarray analysis was performed using Affymetrix GeneChip Mouse Genome 430 2.0 Arrays according to the manufacturer's instructions. Normalization of gene expression data was processed using the Affymetrix Microarray Analysis Suite 5.0 (MAS5) algorithms. Differentially expressed genes were selected with fold change and P value (fold change >2, $P<0.01$). Pathway and gene ontology analyses were performed using the Reactome functional protein interaction database (http://www.reactome.org/).

BMT experiments. BMT was performed as described[39]. In brief, bone marrow cells obtained from *Mincle* KO-*Egfp* Tg mice and *Egfp* Tg mice were washed three times with cold PBS and injected intravenously (1.8×10^6 cells) into 7.5 Gy irradiated 8-week-old male wild-type recipient mice. After 4 weeks, the substitution rate of bone marrow cells was determined by counting EGFP-positive cells in the peripheral blood and then the mice were fed a HFD for 16 weeks.

Statistical analysis. Data are presented as the mean ± s.e.m., and $P<0.05$ and $P<0.01$ were considered statistically significant. Statistical analysis was performed using analysis of variance followed by Tukey–Kramer test. Unpaired t-test was used to compare two groups. In the GTT and ITT data, the entire curves were analysed using repeated-measures analysis of variance adjusted with degrees of freedom by Huynh and Fedlt if the Mauchly's sphericity test is significant ($P<0.05$).

References

1. Hotamisligil, G. S. Inflammation and metabolic disorders. *Nature* **444,** 860–867 (2006).
2. Olefsky, J. M. & Glass, C. K. Macrophages, inflammation, and insulin resistance. *Annu. Rev. Physiol.* **72,** 219–246 (2010).
3. Suganami, T., Tanaka, M. & Ogawa, Y. Adipose tissue inflammation and ectopic lipid accumulation. *Endocr. J.* **59,** 849–857 (2012).
4. Sun, K., Kusminski, C. M. & Scherer, P. E. Adipose tissue remodeling and obesity. *J. Clin. Invest.* **121,** 2094–2101 (2011).
5. Suganami, T., Nishida, J. & Ogawa, Y. A paracrine loop between adipocytes and macrophages aggravates inflammatory changes: role of free fatty acids and tumor necrosis factor alpha. *Arterioscler. Thromb. Vasc. Biol.* **25,** 2062–2068 (2005).
6. Khan, T. *et al.* Metabolic dysregulation and adipose tissue fibrosis: role of collagen VI. *Mol. Cell. Biol.* **29,** 1575–1591 (2009).
7. Jonker, J. W. *et al.* A PPARγ-FGF1 axis is required for adaptive adipose remodelling and metabolic homeostasis. *Nature* **485,** 391–394 (2012).
8. Sun, K., Halberg, N., Khan, M., Magalang, U. J. & Scherer, P. E. Selective inhibition of hypoxia-inducible factor 1α ameliorates adipose tissue dysfunction. *Mol. Cell. Biol.* **33,** 904–917 (2013).
9. Cinti, S. *et al.* Adipocyte death defines macrophage localization and function in adipose tissue of obese mice and humans. *J. Lipid. Res.* **46,** 2347–2355 (2005).
10. Lumeng, C. N., Bodzin, J. L. & Saltiel, A. R. Obesity induces a phenotypic switch in adipose tissue macrophage polarization. *J. Clin. Invest.* **117,** 175–184 (2007).
11. Apovian, C. M. *et al.* Adipose macrophage infiltration is associated with insulin resistance and vascular endothelial dysfunction in obese subjects. *Arterioscler. Thromb. Vasc. Biol.* **28,** 1654–1659 (2008).
12. Bremer, A. A., Devaraj, S., Afify, A. & Jialal, I. Adipose tissue dysregulation in patients with metabolic syndrome. *J. Clin. Endocrinol. Metab.* **96,** E1782–E1788 (2011).
13. Ishikawa, E. *et al.* Direct recognition of the mycobacterial glycolipid, trehalose dimycolate, by C-type lectin Mincle. *J. Exp. Med.* **206,** 2879–2888 (2009).
14. Schoenen, H. *et al.* Cutting edge: Mincle is essential for recognition and adjuvanticity of the mycobacterial cord factor and its synthetic analog trehalose-dibehenate. *J. Immunol.* **184,** 2756–2760 (2010).
15. Wells, C. A. *et al.* The macrophage-inducible C-type lectin, mincle, is an essential component of the innate immune response to *Candida albicans*. *J. Immunol.* **180,** 7404–7413 (2008).
16. Yamasaki, S. *et al.* C-type lectin Mincle is an activating receptor for pathogenic fungus, Malassezia. *Proc. Natl Acad. Sci. USA* **106,** 1897–1902 (2009).
17. Matsumoto, M. *et al.* A novel LPS-inducible C-type lectin is a transcriptional target of NF-IL6 in macrophages. *J. Immunol.* **163,** 5039–5048 (1999).
18. Ichioka, M. *et al.* Increased expression of macrophage-inducible C-type lectin in adipose tissue of obese mice and humans. *Diabetes* **60,** 819–826 (2011).
19. Yamasaki, S. *et al.* Mincle is an ITAM-coupled activating receptor that senses damaged cells. *Nat. Immunol.* **9,** 1179–1188 (2008).
20. Wynn, T. A. & Ramalingam, T. R. Mechanisms of fibrosis: therapeutic translation for fibrotic disease. *Nat. Med.* **18,** 1028–1040 (2012).
21. Hinz, B. *et al.* The myofibroblast: one function, multiple origins. *Am. J. Pathol.* **170,** 1807–1816 (2007).
22. Liu, J. *et al.* Genetic deficiency and pharmacological stabilization of mast cells reduce diet-induced obesity and diabetes in mice. *Nat. Med.* **15,** 940–945 (2009).
23. Mutch, D. M. *et al.* Needle and surgical biopsy techniques differentially affect adipose tissue gene expression profiles. *Am. J. Clin. Nutr.* **89,** 51–57 (2009).
24. Itoh, M. *et al.* Melanocortin 4 receptor-deficient mice as a novel mouse model of nonalcoholic steatohepatitis. *Am. J. Pathol.* **179,** 2454–2463 (2011).
25. Duffield, J. S. *et al.* Selective depletion of macrophages reveals distinct, opposing roles during liver injury and repair. *J. Clin. Invest.* **115,** 56–65 (2005).
26. Itoh, M. *et al.* Hepatic crown-like structure: a unique histological feature in non-alcoholic steatohepatitis in mice and humans. *PLoS ONE* **8,** e82163 (2013).
27. Lipinski, T. *et al.* Enhanced immunogenicity of a tricomponent mannan tetanus toxoid conjugate vaccine targeted to dendritic cells via Dectin-1 by incorporating β-glucan. *J. Immunol.* **190,** 4116–4128 (2013).
28. Takamiya, R., Ohtsubo, K., Takamatsu, S., Taniguchi, N. & Angata, T. The interaction between Siglec-15 and tumor-associated sialyl-Tn antigen enhances TGF-β secretion from monocytes/macrophages through the DAP12-Syk pathway. *Glycobiology* **23,** 178–187 (2013).
29. Shaul, M. E., Bennett, G., Strissel, K. J., Greenberg, A. S. & Obin, M. S. Dynamic, M2-like remodeling phenotypes of CD11c+ adipose tissue macrophages during high-fat diet—induced obesity in mice. *Diabetes* **59,** 1171–1181 (2010).
30. Wentworth, J. M. *et al.* Pro-inflammatory CD11c+CD206+ adipose tissue macrophages are associated with insulin resistance in human obesity. *Diabetes* **59,** 1648–1656 (2010).
31. Zeyda, M. *et al.* Human adipose tissue macrophages are of an anti-inflammatory phenotype but capable of excessive pro-inflammatory mediator production. *Int. J. Obes. (Lond)* **31,** 1420–1428 (2007).
32. Divoux, A. *et al.* Fibrosis in human adipose tissue: composition, distribution, and link with lipid metabolism and fat mass loss. *Diabetes* **59,** 2817–2825 (2010).
33. Bourlier, V. *et al.* TGFbeta family members are key mediators in the induction of myofibroblast phenotype of human adipose tissue progenitor cells by macrophages. *PLoS ONE* **7,** e31274 (2012).
34. Gagnon, A., Yarmo, M. N., Landry, A. & Sorisky, A. Macrophages alter the differentiation-dependent decreases in fibronectin and collagen I/III protein levels in human preadipocytes. *Lipids* **47,** 873–880 (2012).
35. Keophiphath, M. *et al.* Macrophage-secreted factors promote a profibrotic phenotype in human preadipocytes. *Mol. Endocrinol.* **23,** 11–24 (2009).
36. Lê, K. A. *et al.* Subcutaneous adipose tissue macrophage infiltration is associated with hepatic and visceral fat deposition, hyperinsulinemia, and stimulation of NF-κB stress pathway. *Diabetes* **60,** 2802–2809 (2011).
37. Okabe, M., Ikawa, M., Kominami, K., Nakanishi, T. & Nishimune, Y. 'Green mice' as a source of ubiquitous green cells. *FEBS Lett.* **407,** 313–319 (1997).
38. Higashiyama, R. *et al.* Negligible contribution of bone marrow-derived cells to collagen production during hepatic fibrogenesis in mice. *Gastroenterology* **137,** 1459–1466 (2009).
39. Ito, A. *et al.* Role of CC chemokine receptor 2 in bone marrow cells in the recruitment of macrophages into obese adipose tissue. *J. Biol. Chem.* **283,** 35715–35723 (2008).
40. Kitagawa, K. *et al.* Blockade of CCR2 ameliorates progressive fibrosis in kidney. *Am. J. Pathol.* **165,** 237–246 (2004).
41. Murano, I. *et al.* Dead adipocytes, detected as crown-like structures, are prevalent in visceral fat depots of genetically obese mice. *J. Lipid. Res.* **49,** 1562–1568 (2008).
42. Miyake, Y. *et al.* C-type lectin MCL is an FcRγ-coupled receptor that mediates the adjuvanticity of mycobacterial cord factor. *Immunity* **38,** 1050–1062 (2013).
43. Tanaka, M. *et al.* Role of central leptin signaling in the starvation-induced alteration of B-cell development. *J. Neurosci.* **31,** 8373–8380 (2011).
44. Nishimura, S. *et al.* Adipose natural regulatory B cells negatively control adipose tissue inflammation. *Cell Metab.* **18,** 759–766 (2013).
45. Kimura, K. *et al.* Histidine augments the suppression of hepatic glucose production by central insulin action. *Diabetes* **62,** 2266–2277 (2013).
46. Ozeki, Y. *et al.* Macrophage scavenger receptor down-regulates mycobacterial cord factor-induced proinflammatory cytokine production by alveolar and hepatic macrophages. *Microb. Pathog.* **40,** 171–176 (2006).

Acknowledgements

We thank Drs Shizuo Akira and Masaru Okabe, Osaka University, for the generous gift of *Mincle* KO mice and *Egfp* Tg mice, respectively, and Dr Takahisa Nakamura, Cincinnati Children's Hospital Medical Center, for critical reading of the manuscript. This work was supported in part by Grants-in-Aid for Scientific Research from the Ministry of Education, Culture, Sports, Science and Technology of Japan, the Ministry of Health, Labour and Welfare of Japan, and Japan Science and Technology Agency, PRESTO. This work was also supported by research grants from Takeda Medical Research Foundation, The Tokyo Biochemical Research Foundation, Astellas Foundation for Research on Metabolic Disorders, The Mochida Memorial Foundation for Medical and Pharmaceutical Research and The Ichiro Kanehara Foundation.

Author contributions

M.T. and K.I. researched the data, contributed to the discussion and wrote the manuscript. C.K., K.O., I.S., M.H., K.K. and H.I. researched the data. T.M. contributed to cDNA microarray analysis. S.N., I.M., Y.I. and S.A. contributed to the histological analysis. S.Y. contributed to the discussion. T.S. and Y.O. contributed to the discussion and wrote, reviewed and edited the manuscript.

Additional information

Accession codes: Microarray data have been deposited in the NCBI Gene Expression Omnibus (GEO) under accession code GSE52338.

Supplementary Information accompanies this paper at http://www.nature.com/naturecommunications

Competing financial interests: The authors declare no competing financial interests.

Reprints and permission information is available online at http://npg.nature.com/reprintsandpermissions/

How to cite this article: Tanaka, M. *et al.* Macrophage-inducible C-type lectin underlies obesity-induced adipose tissue fibrosis. *Nat. Commun.* 5:4982 doi: 10.1038/ncomms5982 (2014).

PLOS | ONE

RESEARCH ARTICLE

Eicosapentaenoic Acid Ameliorates Non-Alcoholic Steatohepatitis in a Novel Mouse Model Using Melanocortin 4 Receptor-Deficient Mice

Kuniha Konuma[1,2☯], Michiko Itoh[1☯], Takayoshi Suganami[3,4]*, Sayaka Kanai[1], Nobutaka Nakagawa[1], Takeru Sakai[1], Hiroyuki Kawano[5], Mitsuko Hara[6], Soichi Kojima[6], Yuichi Izumi[2], Yoshihiro Ogawa[1,7]

1 Department of Molecular Endocrinology and Metabolism, Graduate School of Medical and Dental Sciences, Tokyo Medical and Dental University, Tokyo, Japan, **2** Department of Periodontology, Graduate School of Medical and Dental Sciences, Tokyo Medical and Dental University, Tokyo, Japan, **3** Department of Organ Network and Metabolism, Graduate School of Medical and Dental Sciences, Tokyo Medical and Dental University, Tokyo, Japan, **4** Japan Science and Technology Agency, PRESTO, Tokyo, Japan, **5** Development Research, Pharmaceutical Research Center, Mochida Pharmaceutical, Shizuoka, Japan, **6** Micro-Signaling Regulation Technology Unit, RIKEN Center for Life Science Technologies, Wako, Japan, **7** Japan Science and Technology Agency, CREST, Tokyo, Japan

☯ These authors contributed equally to this work.
* suganami.mem@tmd.ac.jp

OPEN ACCESS

Citation: Konuma K, Itoh M, Suganami T, Kanai S, Nakagawa N, Sakai T, *et al.* (2015) Eicosapentaenoic Acid Ameliorates Non-Alcoholic Steatohepatitis in a Novel Mouse Model Using Melanocortin 4 Receptor-Deficient Mice. PLoS ONE 10(3): e0121528. doi:10.1371/journal.pone.0121528

Academic Editor: Motoyuki Otsuka, The University of Tokyo, JAPAN

Received: November 13, 2014

Accepted: February 3, 2015

Published: March 27, 2015

Data Availability Statement: All relevant data are within the paper and its Supporting Information files.

Funding: This work was supported in part by Mochida Pharmaceutical Co. Ltd. who also provided highly purified EPA ethyl ester. Grants-in-Aid for Scientific Research from the Ministry of Education, Culture, Sports, Science and Technology of Japan, the Ministry of Health, Labour and Welfare of Japan, Japan Science and Technology Agency, Japan Society for the Promotion of Science, and research grants from Takeda Science Foundation, Mochida Memorial Foundation for Medical and Pharmaceutical

Abstract

Many attempts have been made to find novel therapeutic strategies for non-alcoholic steatohepatitis (NASH), while their clinical efficacy is unclear. We have recently reported a novel rodent model of NASH using melanocortin 4 receptor-deficient (MC4R-KO) mice, which exhibit the sequence of events that comprise hepatic steatosis, liver fibrosis, and hepatocellular carcinoma with obesity-related phenotypes. In the liver of MC4R-KO mice, there is a unique histological feature termed hepatic crown-like structures (hCLS), where macrophages interact with dead hepatocytes and fibrogenic cells, thereby accelerating inflammation and fibrosis. In this study, we employed MC4R-KO mice to examine the effect of highly purified eicosapentaenoic acid (EPA), a clinically available *n*-3 polyunsaturated fatty acid, on the development of NASH. EPA treatment markedly prevented the development of hepatocyte injury, hCLS formation and liver fibrosis along with lipid accumulation. EPA treatment was also effective even after MC4R-KO mice developed NASH. Intriguingly, improvement of liver fibrosis was accompanied by the reduction of hCLS formation and plasma kallikrein-mediated transforming growth factor-β activation. Moreover, EPA treatment increased the otherwise reduced serum concentrations of adiponectin, an adipocytokine with anti-inflammatory and anti-fibrotic properties. Collectively, EPA treatment effectively prevents the development and progression of NASH in MC4R-KO mice along with amelioration of hepatic steatosis. This study unravels a novel anti-fibrotic mechanism of EPA, thereby suggesting a clinical implication for the treatment of NASH.

Research, Ono Medical Research Foundation, Yokoyama Foundation for Clinical Pharmacology, and The Uehara Memorial Foundation. Michiko Itoh was supported by Research Fellowship of Japan Society for the Promotion of Science. Co-author Hiroyuki Kawano is employed by Mochida Pharmaceutical Co. Ltd. Mochida Pharmaceutical Co. Ltd. provided support in the form of salary for Hiroyuki Kawano, but did not have any additional role in the study design, data collection and analysis, decision to publish, or preparation of the manuscript. The specific role of this author is articulated in the 'author contributions' section.

Competing Interests: Hiroyuki Kawano is an employee of Mochida Pharmaceutical Co. Ltd., which funded this study and provided highly purified EPA ethyl ester. There are no other potential conflicts of interest relevant to this article. This does not alter the authors' adherence to PLOS ONE policies on sharing data and materials.

Introduction

Non-alcoholic fatty liver disease (NAFLD) is recognized as a hepatic phenotype of the metabolic syndrome [1]. It encompasses a wide spectrum of liver impairment ranging from benign simple steatosis to non-alcoholic steatohepatitis (NASH), which can lead to cirrhosis and hepatocellular carcinoma [1]. The "two-hit" hypothesis has been proposed as a potential mechanism underlying NASH, in which the first step involves the excessive accumulation of lipids in the liver, thereby sensitizing the liver to the second hits including oxidative stress, lipopolysaccharide, proinflammatory cytokines and adipocytokines [2–4]. However, the precise mechanisms involved in the disease progression from simple steatosis to NASH and hepatocellular carcinoma are still unclear. Accordingly, specific and definitive therapeutic strategies against NASH have not been fully established. It is partly because there are few animal models that reflect the pathophysiology of human NASH.

Recently, we have reported that melanocortin 4 receptor-deficient (MC4R-KO) mice fed high-fat diet develop a liver condition similar to human NASH, which is associated with obesity, insulin resistance and dyslipidemia [5]. MC4R is a seven-transmembrane G protein-coupled receptor that is implicated in the regulation of food intake and body weight [6]. Because MC4R expression is mainly expressed in the hypothalamus and other brain regions [7], it is likely that the hepatic phenotype in MC4R-KO mice results from loss of function of MC4R in the brain, rather than in the liver itself. Accordingly, MC4R-KO mice would provide a novel rodent model with which to investigate the progression from diet-induced hepatic steatosis to NASH. Using this model, we have reported a unique histological structure in the liver termed hepatic crown-like structures (hCLS), in which macrophages surround dead or dying hepatocytes with large lipid droplets [8]. hCLS structurally resembles obesity-induced adipose tissue CLS [8], where sustained interaction between dead adipocytes and macrophages induces adipose tissue inflammation, thereby leading to systemic insulin resistance [9]. Interestingly, the number of hCLS is positively correlated with the extent of liver fibrosis, and myofibroblasts and collagen deposition are observed nearby hCLS [8], suggesting the role of hCLS in the development of NASH. We also detected hCLS in the liver of NAFLD/NASH patients [8]. On the basis of these observations, hCLS may be involved in disease progression from simple steatosis to NASH.

Fish oil rich in *n-3* polyunsaturated fatty acids (PUFAs) such as eicosapentaenoic acid (EPA) or *n-3* PUFAs are clinically effective to treat hypertriglyceridemia. As a molecular mechanism, *n-3* PUFAs improve hepatic lipid metabolism mainly by regulating transcription factors such as peroxisome proliferators-activated receptor α (PPARα) and sterol regulatory element binding protein-1c [10]. In addition, epidemiological and clinical trials have shown that *n-3* PUFAs significantly reduce the incidence of coronary heart disease [11], probably through their pleiotropic effect including an anti-inflammatory property. Given the suppressive effect on hepatic lipid accumulation and inflammation, *n-3* PUFAs could be therapeutically useful to prevent and/or treat NASH. Indeed, recent evidence suggests that *n-3* PUFAs effectively inhibit the development of the diet- or genetically-induced rodent models of NASH, whereas other studies failed [12–17]. However, the recent guideline pointed out that clinical efficacy of *n-3* PUFAs on NAFLD/NASH is controversial [18–25]. Moreover, it is still unclear which species in *n-3* PUFAs are responsible for the treatment of NASH and whether *n-3* PUFAs can regress the hepatic lesion after NASH develops.

In this study, we employed MC4R-KO mice to examine the effect of highly purified EPA on the development of NASH. EPA treatment markedly prevented hepatocyte injury, hCLS formation and collagen deposition along with lipid accumulation in the liver of MC4R-KO mice. Our data also showed that EPA treatment was effective after MC4R-KO mice developed NASH. Intriguingly, the improvement of liver fibrosis was in parallel with the reduction of

hCLS formation and hepatocyte injury, suggesting the involvement of hCLS in the beneficial effect of EPA. Collectively, this study raises a novel anti-fibrotic mechanism of EPA in a mouse model of NASH, thereby suggesting its therapeutic efficacy in NASH.

Methods

Materials

Preparation and characterization of highly purified EPA ethyl ester (purity: >98%, Mochida Pharmaceutical Co., Ltd., Tokyo, Japan) used in animal studies were reported elsewhere [26,27]. Ethyl palmitate (purity > 95%) was purchased from Wako (Tokyo, Japan).

Animals

The MC4R-KO mice on the C57BL/6J background were a generous gift from Dr. Joel K. Elmquist (University of Texas Southwestern Medical Center) [6]. Male C57BL/6J wildtype mice were purchased from CLEA Japan (Tokyo, Japan). The animals were housed in individual cages in a temperature-, humidity- and light-controlled room (12-h light and 12-h dark cycle) and allowed free access to water and standard diet (SD) (CE-2; CLEA Japan). After 1-week acclimation period, 8 week-old male mice were given free access to water and either SD or Western diet (WD) (D12079B; Research Diets, New Brunswick, NJ) supplemented with 5% (wt/wt) ethyl palmitate or EPA ethyl ester [27]. Detailed dietary composition of the SD and WD is shown in S1 Table. All diets were changed every day and served with a non-metallic feeder to prevent oxidization of fatty acids. In this study, we conducted two experimental protocols to evaluate the preventive and therapeutic effect of EPA, *i.e.* EPA treatment throughout the experimental period (24 weeks) and 4-week EPA treatment after the development of NASH, respectively. At the end of the experiments, they were sacrificed, when fed *ad libitum*, under intraperitoneal pentobarbital anesthesia (30 mg/kg). All animal experiments were conducted in accordance to the guidelines for the care and use of laboratory animals of Tokyo Medical and Dental University. The protocol was approved by Tokyo Medical and Dental University Committee on Animal Research (No. 0140016A, No. 2011-207C3).

Blood Analysis

Blood glucose levels were measured by the blood glucose test meter (Glutest PRO R; Sanwa-Kagaku, Nagoya Japan). Serum concentrations of alanine aminotransferase (ALT), triglyceride (TG), free fatty acid (FFA) and total cholesterol (TC) were measured by the respective standard enzymatic assays. Serum concentrations of adipocytokines were determined by the commercially available enzyme-linked immunosorbent assay (ELISA) kits (insulin: Morinaga, Tokyo, Japan; adiponectin: Otsuka Pharmaceutical, Tokyo, Japan; leptin: R&D systems, Minneapolis, MN). For insulin tolerance test, 1-hour fasted mice injected intraperitoneally with human insulin at 1.0 U/kg and blood glucose levels were determined before and at 15, 30, 60, 90 and 120 min after insulin administration.

Hepatic TG Content

Total lipids in the liver were extracted with ice-cold 2:1 (vol/vol) chloroform/methanol. The TG concentrations were measured by an enzymatic assay kit (Wako Pure Chemicals, Osaka, Japan) [5].

Quantification of Active TGFβ1 Content

Active transforming growth factor-β1 (TGFβ1) protein levels in the liver were measured as described [28]. Briefly, frozen liver samples were homogenizes in a lysis buffer (20 mM Tris, pH 7.5, 10 mM ethylenediaminetera-acetic acid) supplemented with protease inhibitors (2 mM phenylmethane sulfonyl fluoride, 0.5 mM dithiothreitol, protease inhibitor cocktail (Sigma, St. Louis, MO)). Samples were centrifuged at 17,000 x g for 20 min at 4°C and the supernatants were subjected to the ELISA kit for mouse TGFβ1 (R&D). Active TGFβ1 protein levels were normalized to the protein concentrations.

Histological Analysis

The liver samples were fixed with neutral-buffered formalin and embedded in paraffin. Four-μm-thick sections were stained with Masson-trichrome and Sirius red [5]. The presence of F4/80-positive macrophages was detected immunohistochemically using the rat monoclonal anti-mouse F4/80 antibody described elsewhere [29]. Proteolytic activation of latent TGFβ was detected with antibody against R58 latency associated protein degradation products (LAP-DPs) [30]. Apoptotic cells were detected by TdT mediated dUTP-biotin nick end labeling (TUNEL) assay using ApopTag Plus Peroxidase In Situ Apoptosis Detection Kit (Millipore, Billerica, MA). The Sirius red-positive and R58 LAP-DP-positive areas were measured using the software WinROOF (Mitani, Chiba, Japan). TUNEL-positive cells were counted in the whole area of each section and expressed as the mean number/mm^2. The liver histology was assessed by two investigators without knowledge of the origin of the slides according to the NASH clinical research network scoring system [31].

Quantitative Real-Time PCR

Total RNA was extracted from the liver using Sepasol reagent (Nacalai Tesque, Kyoto, Japan). Quantitative real-time PCR was performed with StepOnePlus Real-time PCR System using Fast SYBR Green Master Mix Reagent (Applied Biosystems, Foster City, CA) as described previously [5]. Primers used in this study were described in S2 Table. Levels of mRNA were normalized to those of 36B4 mRNA.

Statistical Analysis

Data are presented as mean ± SE, and $P < 0.05$ was considered statistically significant. Statistical analysis was performed using analysis of variance followed by Scheffe's test. Differences between two groups were compared using Student *t*-test. Pearson correlation coefficient was employed to investigate the correlation among the numbers of hCLS and TUNEL-positive cells, and the extent of fibrosis.

Results

Preventive effect of EPA on hepatic lipid accumulation in MC4R-KO mice

First, we examined whether EPA treatment prevents the development of NASH using our mouse model of NASH. Wildtype mice were fed SD (WT-SD) and MC4R-KO mice were fed control diet, WD plus 5% weight palmitate (MC4R-control) or with the diet, in which 5% weight palmitate was replaced to EPA (MC4R-EPA Pre) for 24 weeks (Fig 1A). The amount of food intake was comparable between control and EPA-treated MC4R-KO mice (data not shown). The MC4R-KO mice fed control diet showed accelerated body weight gain relative to

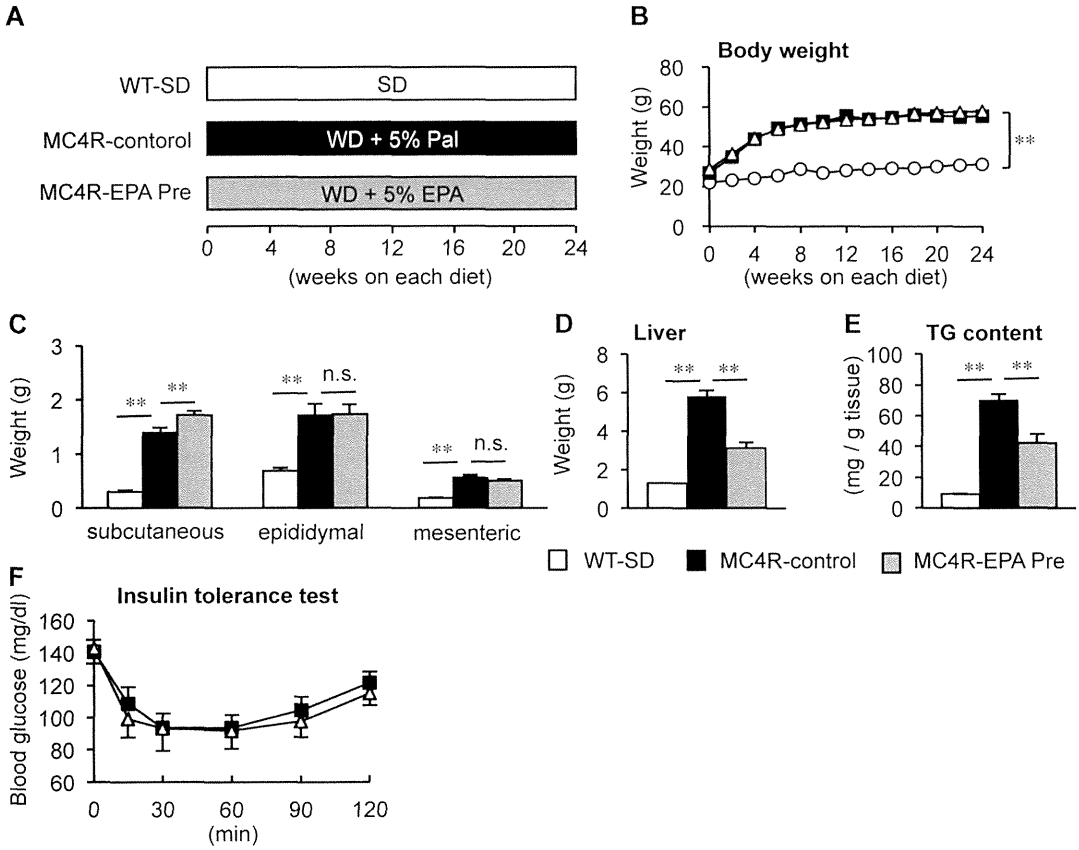

Fig 1. Body weight and tissue weights in MC4R-KO mice treated with EPA for 24 weeks. (A) Experimental protocol of preventive EPA treatment. Growth curve (B) and weights of the subcutaneous, epididymal and mesenteric white adipose tissues (C) and liver (D) of male MC4R-KO (MC4R) and wildtype (WT) mice. WT-SD, WT mice fed standard diet (SD); MC4R-control, MC4R-KO mice fed Western diet (WD) supplemented with 5% (wt/wt) palmitate; MC4R-EPA Pre, MC4R-KO mice fed WD supplemented with 5% (wt/wt) EPA for 24 weeks. Open circle, WT-SD; Open triangle, MC4R-control; closed square, MC4R-EPA Pre. (E) Liver triglyceride (TG) content at 24 weeks. (F) Insulin tolerance test (ITT) at 12-week WD feeding. Open triangle, MC4R-control; closed square, MC4R-EPA Pre. ** $P < 0.01$; n.s., not significant. WT-SD, $n = 8$; MC4R-control, $n = 7$; MC4R-EPA Pre, $n = 10$.

doi:10.1371/journal.pone.0121528.g001

wildtype mice fed SD, along with increased weights of adipose tissue and liver (Fig 1B–1D) as reported [5,8]. EPA treatment showed no appreciable or only marginal effect on body weight and adipose tissue weights (Fig 1B and 1C). On the other hand, the liver weight and the hepatic TG content were markedly reduced in EPA-treated MC4R-KO mice relative to control MC4R-KO mice ($P < 0.01$, Fig 1D and 1E). Hepatic fatty acid composition analysis revealed increased hepatic EPA content and decreased arachidonic acid content (S3 Table). EPA treatment also reduced serum concentrations of TC, FFA, and ALT in MC4R-KO mice, whereas EPA treatment did not affect glucose metabolism and insulin resistance (Table 1, Fig 1F). Since unbalanced production of pro- and anti-inflammatory adipocytokines in obesity has been implicated in the pathogenesis of NASH [32], we examined serum adipocytokine concentrations and found that EPA treatment significantly increased serum adiponectin concentrations in MC4R-KO mice (Table 1). On the other hand, EPA treatment did not affect serum concentrations of leptin in MC4R-KO mice (Table 1).

Table 1. Serological parameters of MC4R-KO and WT mice treated with EPA for 24 weeks.

	WT	MC4R-KO	
	SD	Control	EPA-pre
BG (*ad lib*, mg/dL)	144.0 ± 7.3	134.3 ± 9.7	119.1 ± 6.2
Insulin (*ad lib*, ng/mL)	0.6 ± 0.1	4.3 ± 1.3**	3.7 ± 1.8
TG (mg/dL)	57.1 ± 30.9	30.9 ± 3.2**	34.6 ± 6.0
TC (mg/dL)	70.8 ± 3.0	290.1 ± 15.0**	122.5 ± 8.3¶
FFA (mEq/L)	1.13 ± 0.10	1.33 ± 0.09	0.80 ± 0.05¶
ALT (IU/L)	47.5 ± 5.6	539.1 ± 87.2**	120.5 ± 16.8¶
Adiponectin (μg/mL)	12.7 ± 1.4	7.8 ± 1.0	17.7 ± 2.0¶
Leptin (ng/mL)	8.7 ± 1.8	114.3 ± 4.5**	119.9 ± 8.9

WT, wildtype; SD, standard diet; BG, blood glucose; TG, triglyceride; FFA, free fatty acid; TC, total cholesterol; ALT, alanine aminotransferase. Data are expressed as the mean ± SE.

**$P < 0.01$ vs. WT-SD

¶ $P < 0.01$ vs. MC4R-Control. $n = 7–10$

doi:10.1371/journal.pone.0121528.t001

Effect of EPA on the development of liver fibrosis in MC4R-KO mice

After 24 weeks, the livers from MC4R-KO mice fed control diet exhibited micro- and macrovesicular steatosis, ballooning degeneration, massive infiltration of inflammatory cells and pericellular fibrosis (Fig 2A and 2C) as reported previously [5,8]. On the other hand, steatotic changes and ballooning degeneration were markedly suppressed in EPA-treated MC4R-KO mice (Fig 2A and 2C). The fibrosis score and fibrosis area were also significantly decreased by EPA treatment (Fig 2B and 2D). Although the inflammation score was unchanged, the scores for steatosis and ballooning degeneration were decreased by EPA treatment, so that there was a significant reduction in NAS in EPA-treated MC4R-KO mice relative to control MC4R-KO mice (Fig 2E and 2F). In this study, mRNA expression of genes related to *de novo* lipogenesis (fatty acid synthase (FAS) and stearoyl-CoA desaturase-1 (SCD-1)) and β-oxidation (carnitine palmitoyltransferase 1A (CPT1A)) was markedly increased in the liver of control MC4R-KO mice relative to wildtype mice as reported [5], which was significantly suppressed by EPA treatment (Fig 3A and 3B). There was no apparent change in mRNA expression of proinflammatory genes such as (macrophage marker F4/80 and tumor necrosis factor-α (TNFα)) (Fig 3C). On the other hand, mRNA expression of TGFβ1-target genes such as collagen α1(I) (COL1A1), tissue inhibitor of metalloproteinase-1 (TIMP1) and matrix metalloproteinase-2 (MMP2) was significantly suppressed, although EPA treatment did not affect mRNA expression of TGFβ1 (Fig 3D). These observations, taken together, suggest that EPA treatment effectively prevents the development of liver fibrosis in MC4R-KO mice.

Effect of EPA on hCLS formation and hepatocyte apoptosis in MC4R-KO mice

We have recently reported a unique histological structure or hCLS in the liver of MC4R-KO mice, where dead hepatocytes are surrounded by CD11c-positive macrophages [8]. Our data also suggest that hCLS promotes liver fibrosis during the progression from simple steatosis to NASH [8]. We found that EPA treatment effectively suppresses hCLS formation in MC4R-KO mice (Fig 4A), In this study, the F4/80-positive area was roughly comparable between the treatments (data not shown). Double immunofluorescent staining of F4/80 and CD11c revealed that hCLS-constituting macrophages are positive for CD11c in EPA-treated MC4R-KO mice

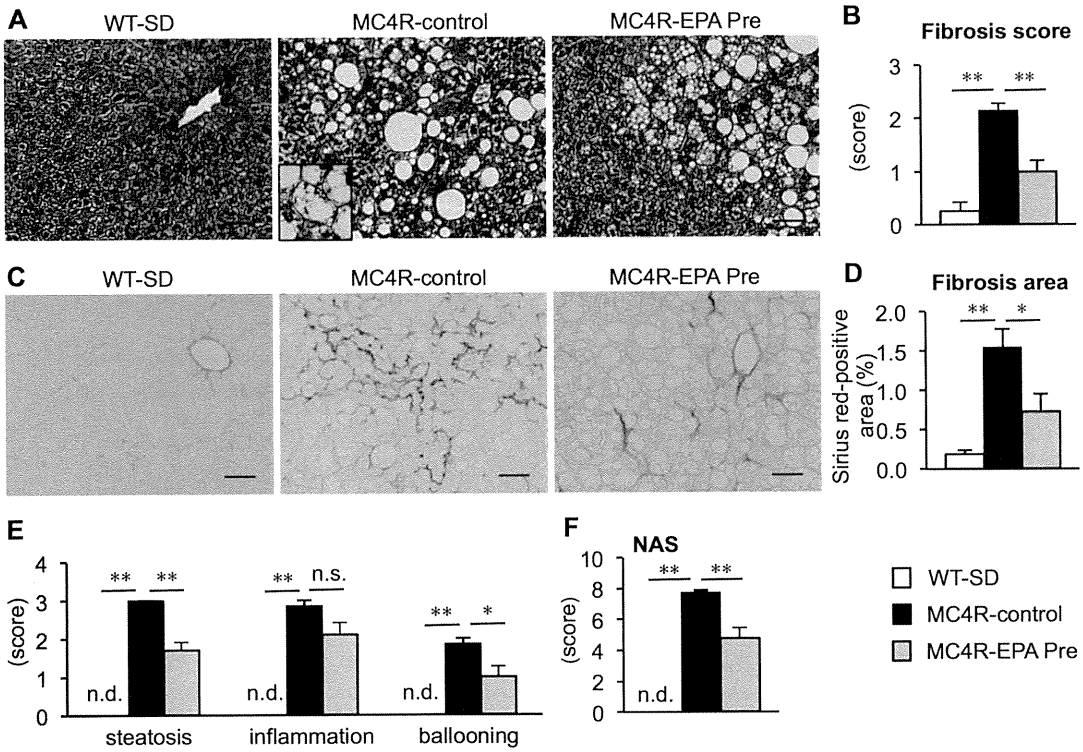

Fig 2. Effect of EPA on liver injury and fibrosis in MC4R-KO mice. Fibrillar collagen deposition evaluated by Masson-trichrome staining (A) and fibrosis scores (B) at 24 weeks. Inset: Representative image of hepatocyte ballooning. Sirius red staining (C) and quantification of Sirius red-positive area (D). Scores of steatosis, lobular inflammation, ballooning degeneration (E) and non-alcoholic fatty liver disease activity score (NAS) (F). Scale bars, 50 μm. * $P < 0.05$; ** $P < 0.01$; n.s., not significant; n.d., not detected. WT-SD, $n = 8$; MC4R-control, $n = 7$; MC4R-EPA Pre, $n = 10$.

doi:10.1371/journal.pone.0121528.g002

(Fig 4B), whereas hepatic mRNA expression of CD11c was significantly suppressed in EPA-treated MC4R-KO mice (Fig 4C) in parallel with reduced number of hCLS. Since hCLS-constituting macrophages are considered to engulf dead hepatocytes and residual lipids [33], we examined apoptotic cells by TUNEL staining. Compared to SD-fed wildtype mice, control MC4R-KO mice showed marked increase in the number of TUNEL-positive cells, most of which assembled around large lipid droplets (Fig 4D). TUNEL-positive cells were decreased in number in EPA-treated MC4R-KO mice relative to control MC4R-KO mice (Fig 4D), which was in parallel with serum ALT concentrations (Table 1). In this study, the number of hCLS was positively correlated with that of TUNEL-positive cells as well as the extent of liver fibrosis (Fig 4E and 4F) [8]. Collectively, these observations suggest that EPA suppresses hepatocyte apoptosis in MC4R-KO mice, which may prevent hCLS formation and fibrotic changes.

Effect of EPA on hepatic TGFβ activation in MC4R-KO mice

Since there was no difference in hepatic TGFβ mRNA expression in MC4R-KO mice between the treatments, we next investigated the TGFβ activation state in the liver. We performed immunostaining using the anti-R58 LAP-DP antibody, which can detect the cleavage site of LAP, serving as a foot print for generation of active TGFβ [30]. The R58 LAP-DP-positive area was increased in the liver of control MC4R-KO mice relative to wildtype mice, which was decreased by EPA treatment (Fig 5A and 5B). The latent TGFβ is activated by plasma kallikrein

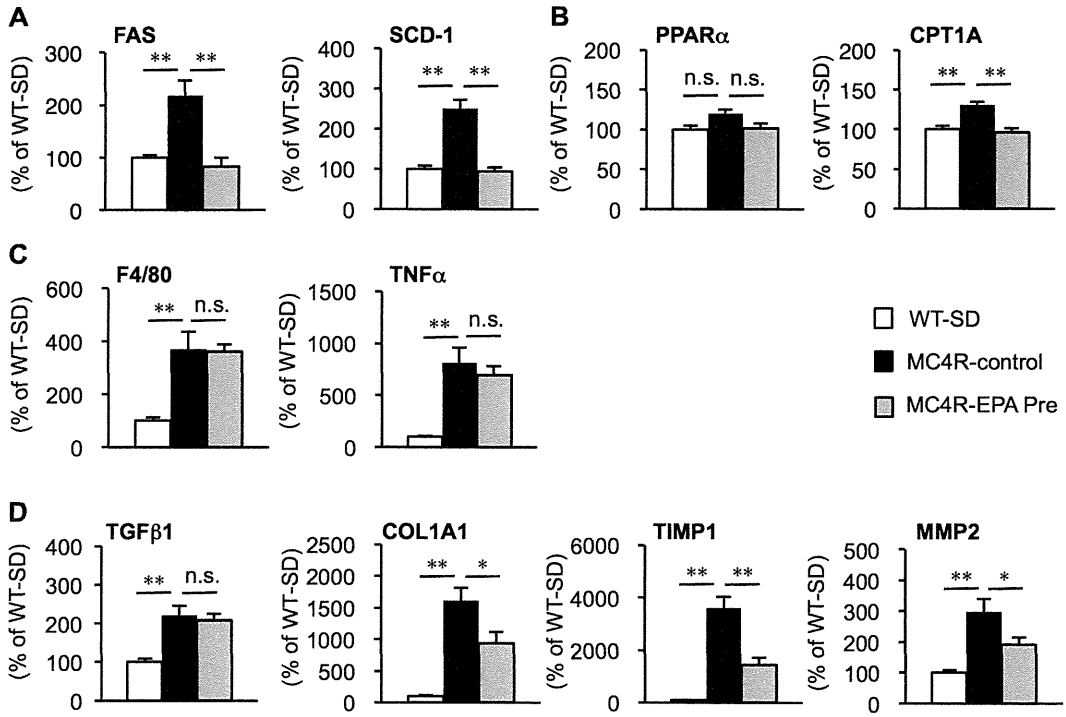

Fig 3. Effect of EPA on hepatic mRNA expression in MC4R-KO mice. Hepatic mRNA expression levels after 24 weeks of EPA treatment. mRNA expression of genes related to *de novo* lipogenesis (fatty acid synthase (FAS) and stearoyl-CoA desaturase (SCD-1)) (A), β-oxidation (peroxisome proliferators-activated receptor α PPARα and carnitine palmitoyltransferase 1A (CTP-1A)) (B), inflammatory markers (F4/80 and tumor necrosis factor α (TNFα) (C) and fibrogenic factors (transforming growth factor β1 (TGFβ1), collagen α1(I) (COL1A1), tissue inhibitor of metalloproteinase-1 (TIMP1) and matrix metalloproteinase-2 (MMP2)) (D). * $P < 0.05$; ** $P < 0.01$; n.s., not significant. WT-SD, $n = 8$; MC4R-control, $n = 7$; MC4R-EPA Pre, $n = 10$.

doi:10.1371/journal.pone.0121528.g003

that is bound to urokinase-type plasminogen activator receptor (uPAR) on the cell surface [34]. In this study, mRNA expression of uPAR was significantly decreased in EPA-treated MC4R-KO mice (Fig 5C). We also confirmed the decreased protein levels of active TGFβ in the liver of EPA-treated MC4R-KO mice (Fig 5D). These observations suggest that EPA suppresses TGFβ activation, thereby inhibiting disease progression from simple steatosis to NASH.

Therapeutic effect of EPA on the progression of NASH in MC4R-KO mice

We also examined whether EPA treatment is effective after 20 weeks of control diet feeding when MC4R-KO mice develop NASH [8]. In this study, MC4R-KO mice were fed either control diet (MC4R-KO control) or EPA-supplemented diet (MC4R-EPA Tx) for another 4 weeks (Fig 6A). The liver weight and hepatic TG content were significantly reduced in EPA-treated MC4R-KO mice relative to control MC4R-KO mice at 24 weeks, whereas body weight and adipose tissue weight except for the epididymal fat depot were unchanged between the groups (S1A–S1D Fig.). Serum concentrations of TC and ALT were reduced, and those of adiponectin were increased in EPA-treated MC4R-KO mice (S4 Table). In this study, histological analysis revealed that EPA treatment for 4 weeks significantly suppressed the progression of liver fibrosis in MC4R-KO mice (Fig 6B–6D). Moreover, the NAS was significantly decreased in EPA-treated MC4R-KO mice relative to control MC4R-KO mice, although the change in each NAS

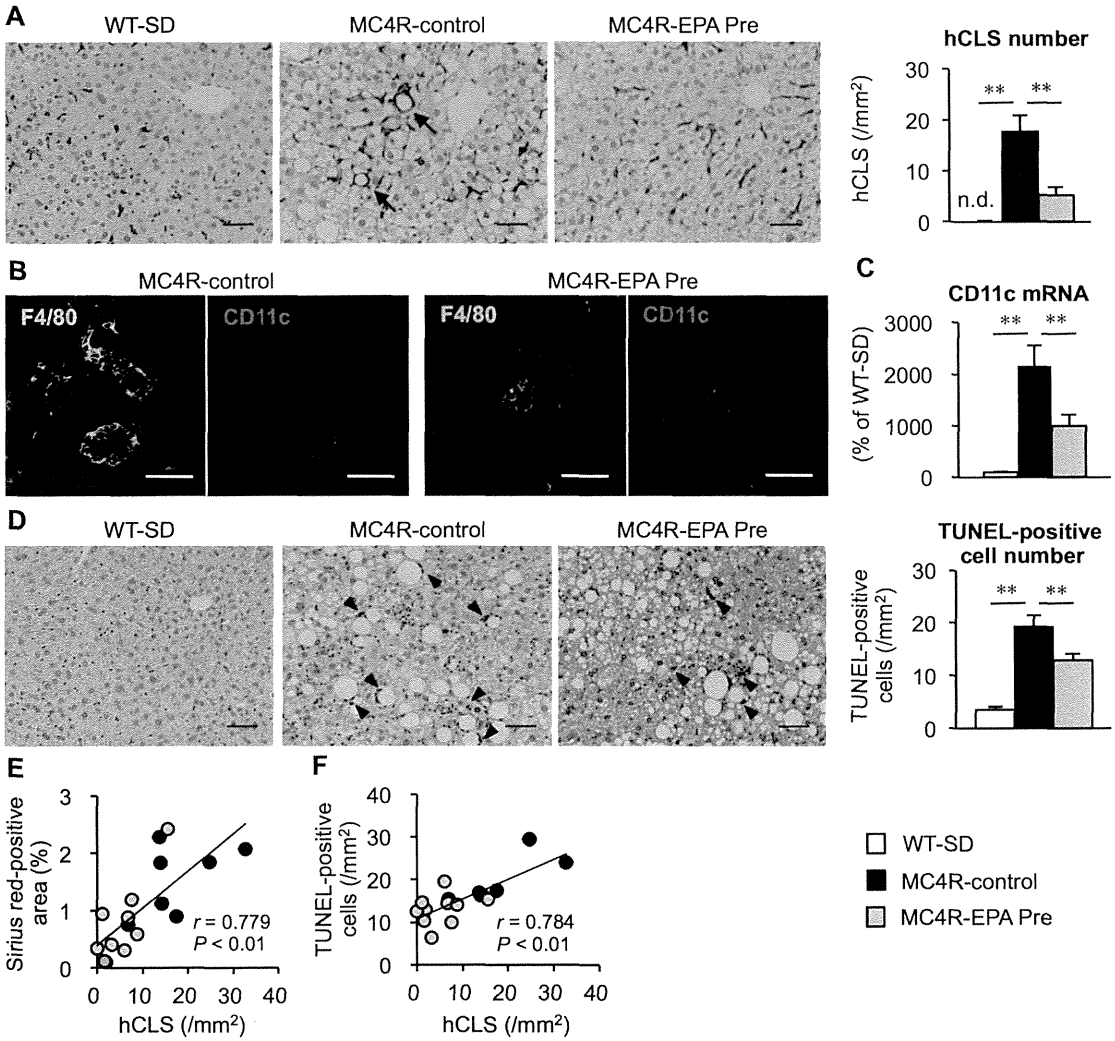

Fig 4. Effect of EPA on hCLS formation and apoptosis in the liver of MC4R-KO mice. (A) F4/80 immunostaining of the liver after 24 weeks of EPA treatment. Arrows indicate characteristic histological features termed "hepatic crown-like structures (hCLS)". (B) Immunofluorescent staining for F4/80 (green) and CD11c (red). (C) Hepatic mRNA expression of CD11c. (D) TdT mediated dUTP-biotin nick end labeling (TUNEL) immunostaining and the number of TUNEL-positive cells. Arrowheads indicate TUNEL-positive cells. Correlation of the number of hCLS and the fibrosis area (E) and the number of TUNEL-positive cells (F). Scale bars, 50 μm. * $P < 0.05$; ** $P < 0.01$; n.d., not detected. WT-SD, $n = 8$; MC4R-control, $n = 7$; MC4R-EPA Pre, $n = 10$.

doi:10.1371/journal.pone.0121528.g004

component (steatosis, inflammation, and ballooning degeneration) did not reach statistic significance (Fig 6E and 6F). Similar to the preventive protocol, hepatic mRNA expression of genes related to *de novo* lipogenesis, β-oxidation, and fibrogenesis was decreased in EPA-treated MC4R-KO mice relative to control MC4R-KO mice (S2 Fig.). The number of hCLS was also significantly reduced in EPA-treated MC4R-KO mice relative to control MC4R-KO mice, along with down-regulation of CD11c mRNA expression (S3A–S3D Fig.). Furthermore, EPA treatment resulted in a significant reduction in the number of TUNEL-positive cells and TGFβ activation (S3E–S3H Fig.). These observations, taken together, suggest that EPA suppressed the progression of liver fibrosis in MC4R-KO mice after the mice developed NASH.

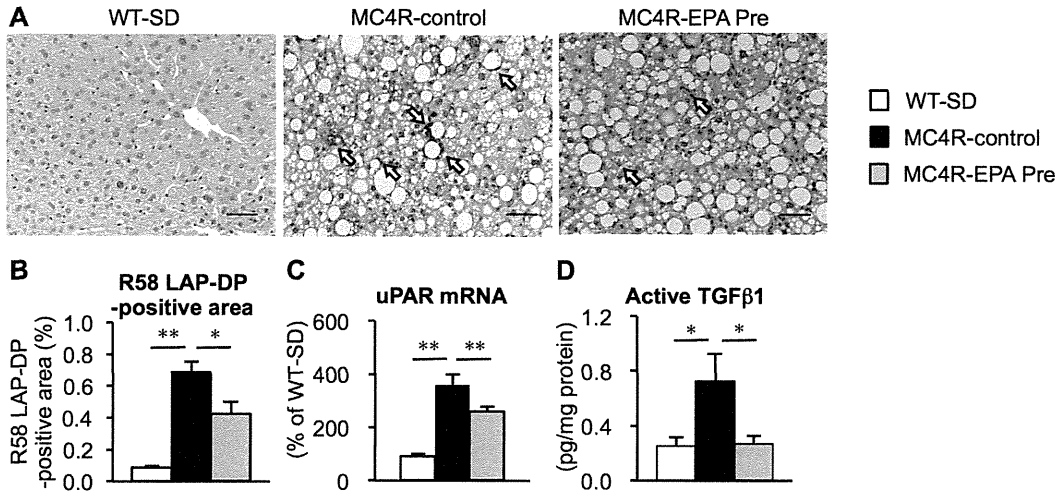

Fig 5. Effect of EPA on hepatic TGFβ activation in MC4R-KO mice. (A) Immmunostaining with anti-R58 LAP-DP antibody to determine TGFβ activation in the liver after 24 weeks of EPA treatment. (B) Quantification of the R58 LAP-DP-positive area. (C) Hepatic mRNA expression of urokinase-type plasminogen activator receptor (uPAR). (D) Active TGFβ protein levels in the liver. Scale bars, 50 μm. * $P < 0.05$; ** $P < 0.01$. WT-SD, $n = 8$; MC4R-control, $n = 7$; MC4R-EPA Pre, $n = 10$.

doi:10.1371/journal.pone.0121528.g005

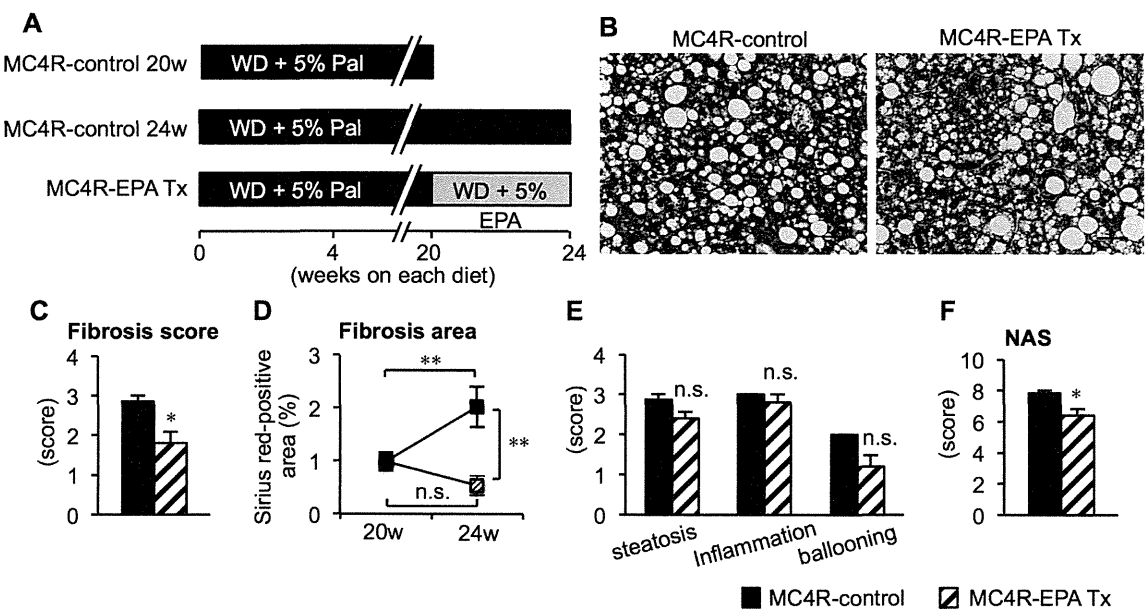

Fig 6. Histological analysis of the liver of MC4R-KO mice treated with EPA for 4 weeks after the development of NASH. (A) Experimental protocol of therapeutic EPA treatment. Fibrillar collagen deposition evaluated by Masson-trichrome staining (B) and fibrosis scores (C). (D) Quantification of Sirius red-positive area. Scores of steatosis, lobular inflammation, ballooning degeneration (E) and NAS (F). Scale bars, 50 μm. * $P < 0.05$; ** $P < 0.01$; n.s., not significant. MC4R-control, $n = 7$; MC4R-EPA Pre, $n = 10$.

doi:10.1371/journal.pone.0121528.g006

Discussion

Using a variety of animal models through genetic, dietary, and/or pharmacologic approaches, many attempts have been made to identify novel therapeutic strategies for NASH, while their clinical efficacy is still unclear. It is partly because of the limited availability of appropriate animal models that reflect a liver condition of human NASH [35]. For instance, dietary deficiency of methionine and choline develops steatosis and mild fibrosis in the liver, although without obesity and insulin resistance [35]. Since NASH is considered as the hepatic phenotype of the metabolic syndrome, crosstalk among multiple organs should be involved in the pathophysiology of NASH. In this regard, MC4R-KO mice, a unique rodent model of NASH accompanied by obesity and systemic insulin resistance, would be useful for evaluating the effectiveness of novel drugs to treat NASH. This is the first report to evaluate drug efficacy using MC4R-KO mice. In this study, we demonstrate that EPA treatment effectively suppresses the development and progression of liver fibrosis along with marked reduction of hepatic steatosis, without affecting body weight. These observations suggest a clinical implication of EPA for the treatment of NASH.

We previously reported that hCLS plays an important role in the progression from simple steatosis to NASH [8]. Since EPA treatment markedly suppressed hCLS formation as well as interstitial fibrosis in MC4R-KO mice, it is likely that one site of actions of EPA is hCLS. Given that CD11c-positive macrophages surround dead hepatocytes in hCLS, EPA may suppress hepatocyte injury and cell death. This notion is supported by our observations that EPA treatment effectively prevented the increase in the number of TUNEL-positive cells, serum ALT concentrations, and the hepatocyte injury score (ballooning) in MC4R-KO mice. Moreover, these effects were observed even when MC4R-KO mice were treated with EPA after NASH developed. During the development of NASH, hepatocytes store excessive lipid including toxic lipids (*i.e.* saturated free fatty acid, free cholesterol, and lysophosphatidyl choline), which leads to metabolic stress such as oxidative stress and endoplasmic reticulum stress, thereby activating the cell death program [1,36,37]. Notably, hepatocyte apoptosis is a prominent feature of human NASH as well [38]. In this regard, it is known that that *n-3* PUFAs can induce gene expression of ROS-degrading enzymes to inhibit oxidative stress, and antagonize the saturated fatty acid-induced endoplasmic reticulum stress [39,40]. It is, therefore, conceivable that EPA treatment ameliorates lipotoxicity of hepatocytes to prevent the formation of hCLS in MC4R-KO mice.

Fibrogenesis is a complex process that involves a variety of cells including both parenchymal cells and stromal cells like myofibroblasts and immune cells. Although EPA and *n-3* PUFAs are known to exert an anti-inflammatory property [10,41], EPA treatment did not affect the inflammation score and TNFα mRNA expression in the liver from MC4R-KO mice. TGFβ, a key regulator of fibrogenesis, is produced as a latent complex containing latency-associated protein and latent TGFβ binding protein, and then activated when released from the latent complex [30]. In this study, expression of uPAR, a cell surface receptor for plasma kallikrein, was increased in the liver of MC4R-KO mice, suggesting the plasma kallikrein-mediated TGFβ activation. Intriguingly, uPAR expression and active TGFβ levels were markedly suppressed by EPA treatment. Among several molecules that can activate TGFβ such as integrins, metalloproteinases and plasmin, plasma kallikrein plays an important role in animal models of liver fibrosis [34,42]. Since TNFα potently induces uPAR expression in cultured hepatic stellate cells [34], it is interesting to know how hCLS formation induces TGFβ activation during the development of NASH and how EPA suppresses the process.

We previously reported that complex interactions between adipose tissue and liver should play a role in the development of NASH in MC4R-KO mice [5]. For instance, unbalanced

production of pro- and anti-inflammatory adipocytokines in obesity has been implicated in the pathogenesis of obesity-related complications including NASH [43]. Among numerous adipocytokines, there is substantial evidence on the protective role of adiponectin in the development of hepatic fibrosis and inflammation [44,45]. As a possible mechanism, adiponectin stimulates β-oxidation by activation of AMP-activated protein kinase and PPARα and down regulates expression of sterol regulatory element binding protein-1c to suppress *de novo* lipogenesis in the liver [46,47]. Adiponectin also exerts its inhibitory effect on platelet-derived growth factor BB- and TGFβ-induced proliferation and migration of hepatic stellate cells [48]. In this study, EPA treatment effectively increased the otherwise reduced serum adiponectin concentrations in MC4R-KO mice, which may be involved in the beneficial effect of EPA on liver injury. As we and others reported previously, serum adiponectin concentrations are elevated in obese mice and humans when treated with EPA or *n-3* PUFA-rich fish oil [26,49,50]. Moreover, we have provided evidence that EPA increases adiponectin secretion through the improvement of obesity-induced adipose tissue inflammation [26]. Neschen *et al.* also showed that fish oil activates PPARγ in adipocytes to increase adiponectin secretion [49]. On the other hand, EPA treatment did not show the effect on the serum concentrations of leptin in MC4R-KO mice, while it is known that leptin promotes liver fibrosis in certain liver fibrosis models [28,51,52]. Collectively, adipose tissue may contribute to the pathogenesis of liver fibrosis in MC4R-KO mice. It is, therefore, conceivable that the beneficial effect of EPA on liver injury of MC4R-KO mice is attributed to its action on adipose tissue as well as liver.

Clinical efficacy of *n-3* PUFAs for the treatment of NAFLD/NASH is still controversial. Tanaka *et al.* reported that highly purified EPA treatment improves biochemical and histological abnormalities in Japanese patients with NASH [21]. In contrast, a recent randomized, double-blind, placebo-controlled trial failed to prove the effectiveness of EPA for 12 months on hepatic steatosis and liver fibrosis in patients with NAFLD/NASH [22,23]. It is noteworthy that the dosage of EPA used in this study might not be enough for American population, where the well-established beneficial effect of EPA on dyslipidemia was not observed [22,23]. There was also no significant improvement in liver histology in several clinical trials using *n-3* PUFAs, in which the treatment showed only marginal effect on dyslipidemia [23–25]. Therefore, additional studies are required regarding the dosage of EPA and duration of the treatment. Moreover, dietary saturated fatty acid composition may affect the efficacy of EPA treatment, since experimental evidence in rodents suggest that EPA exerts its anti-inflammatory property, at least in part, through counteracting saturated fatty acids [26], and diet rich in saturated fatty acids augments insulin resistance and NAFLD [53,54]. Based on the heterogeneity of NAFLD/NASH patients, it is also important to evaluate the effect of EPA in subgroups with differential risk factors.

In conclusion, we demonstrate that EPA treatment effectively prevents the development and progression of liver fibrosis in MC4R-KO mice along with marked reduction of hepatic steatosis. EPA may exert its anti-fibrotic effect through suppression of hepatocyte injury-induced TGFβ activation in hCLS. Our data also suggest that EPA acts on adipose tissue as well as liver to ameliorate liver fibrosis. This study unravels a novel anti-fibrotic mechanism of EPA, thereby suggesting a clinical implication for the treatment of NASH.

Supporting Information

S1 Fig. Body weight and tissue weights in MC4R-KO mice in the therapeutic study. Body weight (A) and weights of the subcutaneous, epididymal, and mesenteric white adipose tissues (B) and liver (C) of male MC4R-KO before EPA treatment (Western diet (WD) supplemented with 5% (wt/wt) palmitate for 20 weeks) and after 4-week EPA treatment. MC4R-EPA Tx,